

## 27. Dark Matter

Revised August 2023 by L. Baudis (Zurich U.) and S. Profumo (UC Santa Cruz).

### 27.1 The case for dark matter

Modern cosmological models invariably include an electromagnetically close-to-neutral, non-baryonic matter species with negligible velocity from the standpoint of structure formation, generically referred to as “cold dark matter” (CDM; see The Big-Bang Cosmology—Sec. 22 of this *Review*). For the benchmark  $\Lambda$ CDM cosmology adopted in the Cosmological Parameters—Sec. 25 of this *Review*, the DM accounts for 26.4% of the critical density in the universe, or 84.4% of the total matter density. The nature of only a small fraction, between at least 0.5% (given neutrino oscillations) and at most 1.6% (from combined cosmological constraints), of the non-baryonic matter content of the universe is known: the three Standard Model neutrinos (see the Neutrino Masses, Mixing, and Oscillations—Sec. 14 of this *Review* ). The fundamental makeup of the large majority of the DM is, as of yet, unknown.

Assuming the validity of General Relativity, DM is observed to be ubiquitous in gravitationally collapsed structures of size ranging from the smallest known galaxies [1] to galaxies of size comparable to the Milky Way [2], to groups and clusters of galaxies [3]. The mass-to-light ratio is observed to saturate at the largest collapsed scales to a value indicative, and close to, what inferred from other cosmological observations for the universe as a whole [4]. In such collapsed structures, the existence of DM is inferred directly using tracers of mass enclosed within a certain radius such as stellar velocity dispersion, rotation curves in axisymmetric systems, the virial theorem, gravitational lensing, and measures of the amount of non-dark, i.e. baryonic, mass such as stellar number counts and tracers of gas density such as X-ray emission [5]. The global DM abundance as determined from cosmological probes is discussed in Sec. 22.

The picture of structure formation in modern cosmology heavily relies on, and can be considered an independent and exceptionally strong motivation for, DM. Baryonic density fluctuations at CMB decoupling are observed to be at most on the order of  $\delta\rho_b/\rho_b|_{\text{rec}} \approx 10^{-5}$ ; since density perturbations grow linearly with the scale factor in the linear regime, absent any other matter fluid, one would predict that

$$\delta\rho_b/\rho_b|_{\text{today}} \approx \frac{\delta\rho_b/\rho_b|_{\text{rec}}}{a_{\text{rec}}} \approx 10^{-2}, \quad (27.1)$$

at odds with the observed highly non-linear structures in the universe,  $\delta\rho_b/\rho_b|_{\text{obs}} \gg 1$ . The presence of a dominant non-relativistic (“cold”) pressure-less matter component decoupled from the thermal bath well before recombination allows instead for the prediction of a matter power spectrum in remarkable agreement with observations [6].

Assuming deviations of gravitational interactions on large scales from general relativity or from its Newtonian limit, certain effects, attributed in the standard scenario to DM, can be explained by modified gravity [7]. Usually such theories mimic the effects otherwise attributed to DM on a limited range of scales, but fail globally, and especially at the largest scales. Key issues that at present appear highly problematic in the framework of theories of modified gravity without DM include (i) predicting the correct spectrum of density perturbations, (ii) predicting the observed anisotropy power spectrum of the CMB, and (iii) explaining weak lensing and X-ray observations of merging clusters such as 1E 0657-558 (the “Bullet” cluster) [8]. The inferred relative speed of gravitational and electromagnetic radiation in GW170817 additionally excludes a significant swath of modified theories of gravity where the two speeds (of gravitational and electromagnetic waves) differ [9].

## 27.2 Properties of dark matter candidates

**Electric charge:** The “darkness” of DM can be quantified based on constraints from the CMB and large-scale structure: if the DM is charged, or “milli-charged” (for instance via a kinetic mixing with a dark photon field, producing an effective suppressed coupling to the visible photon field), it might impact the baryon-photon plasma during recombination; in turn, DM density fluctuations can be suppressed by radiation pressure and photon diffusion, additionally altering the baryon acoustic peak structure. [10] finds that the most stringent constraints stem from the requirement that the DM be completely decoupled from the baryon-photon plasma at recombination, yielding a maximal “milli-electric” charge, in units of the electron charge, of  $3.5 \times 10^{-7} (m_{\text{DM}}/1 \text{ GeV})^{0.58}$  for  $m_{\text{DM}} > 1 \text{ GeV}$ , and of  $4.0 \times 10^{-7} (m_{\text{DM}}/1 \text{ GeV})^{0.35}$  for  $m_{\text{DM}} < 1 \text{ GeV}$ . Limits also exist from structure formation on how optically dark and dissipationless the DM should be.

**Self-interactions:** Observations of merging clusters [8] and of the ellipticity of certain galaxies as inferred from X-rays [11] constrain the level of DM-DM self interactions. The figure of merit is the ratio of the DM-DM cross section and the DM mass [12] (see Ref. [13] for a review),  $\sigma_{\text{DM-DM}}/m_{\text{DM}} < 0.47 \text{ cm}^2/\text{g} \simeq 0.84 \text{ barn/GeV}$  at 95% C.L.. Assuming a velocity dependence in  $\sigma_{\text{DM-DM}}$ , “self-interacting DM” has been advocated as a possible solution to certain possible small-scale structure issues in the standard non-collisional ( $\sigma_{\text{DM-DM}} \simeq 0$ ) setup [13, 14] (see Sec. 27.4).

**Mass: Lower Limits:** Model-independent lower limits for very small DM masses are due to quantum effects: for fermionic DM particles, the phase-space density  $f(\vec{x}, \vec{p})$  is bounded from above due to Pauli’s exclusion principle,  $f < gh^{-3}$ , with  $g$  the number of internal degrees of freedom and  $h$  Planck’s constant; observations of the velocity dispersion (or, equivalently, measures of the enclosed mass) and physical density in dwarf galaxies, lead to a lower limit on fermionic DM masses, sometimes known as the Tremaine-Gunn limit [15]. Using the Fornax dwarf, Ref. [16] finds  $m_F > 70 \text{ eV}$ . More stringent limits can be drawn from Lyman- $\alpha$  observations, although such limits depend on the thermal history of the DM. In the case of bosonic DM, the Compton wavelength of an ultra-light species might erase small-scale structure, in conflict with CMB and large-scale structure [17], Lyman- $\alpha$  observations [18, 19], and measurements of high-redshift galaxy luminosity functions and the Milky Way satellite luminosity function [20–22]: these observations indicate that  $m_B \gtrsim 10^{-22} \text{ eV}$ .

**Mass: Upper Limits:** General upper limits exist on the mass of the DM constituent from the stability against tidal disruption of structures immersed in DM halos, such as galactic disks and globular clusters, and of individual small galaxies. The most stringent limits can be derived using wide halo binaries [23] and the stability of the star cluster within Eridanus II [24]. Such limits constrain an individual, point-like DM constituent, assuming it makes up 100% of the DM, to be lighter than around  $5 M_\odot$ . (Notice that the mass limits discussed here do not assume any specific production mechanism, and do not depend on the observed cosmological DM density).

**Stability:** The DM lifetime must be long compared to cosmological timescales [25].

## 27.3 Genesis of dark matter

The generation of DM in the early universe can proceed via thermal or non-thermal production, or both, or it may result from a particle-antiparticle asymmetry.

**Freeze-out:** The process of chemical decoupling from the high-temperature, high-density thermal bath (freeze-out) as a paradigm for particle production in the early universe is both a predictive and a successful one. The possibility that just like light elements, neutrinos, and CMB photons, particle DM also originated from a thermal decoupling process has thus garnered significant attention.

A particle species *chemically* decouples when the rate  $\Gamma$  for the species’ number-changing processes drops below the Hubble rate  $H$ . Rough estimates for the abundance of relics can be ob-

tained by (i) calculating the freeze-out (i.e. “decoupling”) temperature  $T_{\text{f.o.}}$ , corresponding to  $H(T_{\text{f.o.}}) \sim \Gamma(T_{\text{f.o.}})$ , (ii) equating the comoving number density at freeze-out and today, eventually (iii) obtaining the physical density of relic particles today. This procedure assumes that entropy is conserved between  $T_{\text{f.o.}}$  and today, an assumption that could well be violated, especially for heavy relics that decouple early, for instance by entropy injection episodes [26]. Notice also that the freeze-out calculation strongly depends on the assumed background cosmology, and changes e.g. if the early universe is not radiation-dominated around DM decoupling.

The calculation of the freeze-out relic abundance hinges on a Boltzmann equation relating the Liouville operator to the collision operator acting on the phase space density. Under a variety of simplifying assumptions including homogeneity and isotropy, it is possible to reduce the relevant equation for the number density  $n$  of a single species pair-annihilating with particles in the thermal bath via 2-to-2 processes to

$$\frac{dn}{dt} - 3Hn = -\langle\sigma v\rangle (n^2 - n_{\text{eq}}^2), \quad (27.2)$$

where  $\langle\sigma v\rangle$  is the thermally-averaged pair-annihilation cross section times relative velocity (see Ref. [27]), and  $n_{\text{eq}}$  is the equilibrium number density. Relics for which the freeze-out temperature is much larger than the particle mass (and thus that freeze-out as ultra-relativistic) are called *hot* relics; if the opposite is true, the relic is instead considered *cold*.

A straightforward calculation shows that to leading order the frozen-out density of *hot* relics is *linearly proportional to the relic particle mass*. The comoving number density  $Y = n/s$ , where  $s$  is the entropy density, for a hot relic is approximately given by its equilibrium value,

$$Y_{\text{f.o.}} \simeq Y_{\text{eq}} \simeq 0.278 \frac{g_{\text{eff}}}{g_{*s}}, \quad (27.3)$$

where  $g_{\text{eff}}$  is the relic’s effective number of degrees of freedom, and  $g_{*s}$  is the number of entropic relativistic degrees of freedom, both calculated at  $T_{\text{f.o.}}$ . The resulting relic abundance, assuming an iso-entropic expansion, is

$$\Omega_{\text{hot}} h^2 = \frac{m Y_{\text{f.o.}} s_0 h^2}{\rho_c} \simeq \frac{m}{93 \text{ eV}}, \quad (27.4)$$

with  $s_0$  the entropy density today, and with the latter equality holding for the case of SM neutrinos, with a freeze-out temperature around 1 MeV (which enters in the final relic abundance through the degrees of freedom dependence on the right-hand-side of Eq. (27.3)).

For *cold* relics, the leading-order dependence of the relic abundance on the DM particle properties is an *inverse proportionality relation to the pair-annihilation cross section*,

$$\Omega_{\text{cold}} h^2 \simeq 0.1 \left( \frac{x_{\text{f.o.}}}{20} \right) \left( \frac{10^{-8} \text{ GeV}^{-2}}{\sigma_{\text{DM+DM}\leftrightarrow\text{anything}}} \right), \quad (27.5)$$

where  $x \equiv m_{\text{DM}}/T$ . In turn, the freeze-out temperature is approximately given by the solution to the equation

$$\sqrt{x} \cdot e^{-x} = (m_{\text{DM}} \cdot M_P \cdot \sigma_{\text{DM+DM}\leftrightarrow\text{anything}})^{-1}, \quad (27.6)$$

where  $M_P \simeq 2.435 \times 10^{18} \text{ GeV}$  is the reduced Planck mass. As a result,  $T_{\text{f.o.}} \simeq m_{\text{DM}}/x_{\text{f.o.}}$ , with  $x_{\text{f.o.}}$  a number between 10 and 50, depending on the cross section, with only a logarithmic dependence on the DM mass. Since for electroweak-scale cross sections and masses  $\sigma_{\text{DM+DM}} \simeq 10^{-8} \text{ GeV}^{-2}$ , “weakly-interacting massive particles”, or WIMPs have gained exceptional popularity. Notice that Eq. (27.5) bears, however, no connection to the weak scale [28], despite the relation being known as “WIMP miracle”.

Numerous scenarios exist, including notably supersymmetry [29, 30] and models with universal extra dimensions [31, 32] where the relic abundance of the DM is controlled by processes involving a slightly heavier, unstable, co-annihilating species [33]. In this case the calculation of the abundance of the stable species proceeds similarly to what outlined above, with an effective pair-annihilation cross section that captures the effects of co-annihilation replacing the pair-annihilation cross section [30].

**Freeze-in:** Collisional processes can lead to the production of out-of-equilibrium particles that progressively accumulate over cosmic time, a process sometimes called *freeze-in*. The abundance of the frozen-in particles produced at a given redshift depends on the product of the production rate times the Hubble time at that redshift. Freeze-in generally implies that the lightest observable-sector particles decay to the DM with relatively long lifetimes, giving peculiar signals at colliders (see e.g. [34]). Gravitinos are an example of DM candidates possibly produced via a freeze-in type scenario, albeit the portal coupling is in that case via a higher dimensional, Planck-suppressed operator [35].

**Cannibalization and other dark-sector number-changing processes:** Thermal processes can drive the abundance of the DM beyond simple 2-to-2 number-changing interactions. For instance, DM can “cannibalize” [36, 37] itself if  $n \rightarrow 2$  processes exist. In this case, a critical aspect is whether or not the DM sector is in thermal contact with the Standard Model thermal bath. If it is,  $n \rightarrow 2$  processes can drive the relic abundance, e.g. in the Strongly Interacting Massive Particles (SIMP) scenario [38]. Models exist where the *kinetic decoupling* (i.e. the decoupling from the *thermal equilibrium velocity distribution*) of the two sectors drives the abundance of the DM (elastically decoupling relics, or ELDERs [39]). When the two sectors are not in thermal contact,  $n \rightarrow 2$  processes heat the DM sector dramatically, rapidly affecting the temperature ratio between the visible and dark sectors [36, 38]. If the relevant cross sections are large enough, and the DM mass light enough, significant effects can arise in structure formation [36].

**Non-thermal production:** DM production can proceed via processes out of thermal equilibrium (“non-thermal” production). These include DM production via the decay of a “mother” particle [40, 41] (or of topological defects [42], moduli [43] etc.) to the DM, or production via gravitational effects.

**Asymmetric DM:** An enticing alternative possibility for DM production is that of *asymmetric* DM [44, 45]: the relic DM abundance arises from an asymmetry between anti-DM and DM. This asymmetry may or may not be related to the baryon-antibaryon asymmetry. If it is, then depending on the model and its thermal history, a relation exists between the mass of the DM and the proton mass. A variety of proposals have been put forward where alternately baryogenesis is explained from a DM sector asymmetry, or vice-versa (see e.g. Ref. [46] for a review).

**Primordial Black Holes production:** A qualitatively stand-alone class of DM candidates, primordial black holes (PBHs), arises from entirely different mechanisms from what reviewed above. PBHs are thought to originate from gravitational collapse of large density fluctuations in the early universe [47, 48]. The over-densities could be produced in a variety of ways, such as topological defects like cosmic strings, necklaces or domain walls, curvature fluctuations from a period of ultra-slow-roll, a sound speed “resonance”, an early phase of matter domination, or sub-horizon phenomena including a phase transition and preheating. Albeit the calculation depends on the details of gravitational collapse, the formation time is connected to the PBH mass via  $M = \gamma M_{PBH} \simeq 2 \times 10^5 \gamma (\frac{t}{s}) M_\odot$ , with  $\gamma \simeq (1/\sqrt{3})^3$  during radiation domination [49].

## 27.4 Density and velocity distribution of dark matter

### 27.4.1 Local density and velocity distribution

The density and distribution of DM in the Milky Way encipher relevant dynamical information about our Galaxy, and are particularly important for direct and indirect detection experiments. The *local density* ( $\rho_0$ ) is an average over a volume of a few hundred parsecs in the Solar neighbourhood.

To determine the local density from observations, two classes of methods are used [50]. So-called *local measures* rely on the vertical motion of tracer stars in the vicinity of the Sun, while *global measures* extrapolate  $\rho_0$  from the measured rotation curve, with additional assumptions about the Galactic halo shape. Conversely, by comparing the extrapolated local density with the one obtained from local measures, one can constrain the local shape of the Milky Way halo. A major source of uncertainty on  $\rho_0$  is the contribution of baryons (stars, gas, stellar remnants) to the local dynamical mass. For instance, the motion of tracer stars used in local measures is dictated by the total potential generated by baryons and DM, and a robust baryonic census must be available to infer the additional contribution from DM. Recent determinations from global methods lie in the range  $(0.2 - 0.6)$  GeV/cm<sup>3</sup>, while new studies of the local DM density from *Gaia* satellite data yield  $(0.3 - 1.5)$  GeV/cm<sup>3</sup>, depending on the type of stars used in the study.

Other observational quantities that enter in the phase space distribution of DM, and provide constraints on mass models of the Milky Way are the local circular speed  $v_c$  and the escape velocity  $v_{esc}$ . The local circular speed is measured by various methods, roughly divided into measurements of the Sun's velocity with respect to an object assumed to be at rest with respect to the Galactic centre or direct measurements of the local radial force. These methods yield values of  $v_c = (218 - 246)$  km/s. A recent estimate of the escape velocity, defined as the speed above which objects are not gravitationally bound to our galaxy, is  $v_{esc} = 533^{+54}_{-41}$  km/s [51] (see also the more recent estimate in [52] of  $v_{esc} = 484.6^{+17.8}_{-7.4}$  km/s, which is not in tension with the value we use).

The local velocity distribution of DM particles can not be measured directly at present, and is mostly derived from simulations. In general, experiments use the simplest, so-called *Standard Halo Model (SHM)* for their data analysis. It assumes an isotropic, isothermal sphere of DM particles with a density profile of  $\rho(r) \propto r^{-2}$ , for which the velocity distribution is Maxwellian, with a velocity dispersion  $\sigma_v = v_c/\sqrt{2}$ . This distribution, which formally extends to infinity, is truncated at  $v_{esc}$  [53]. Earlier high resolution, dark-matter-only simulations found velocity distributions that markedly deviated from a Maxwell-Boltzmann distribution and in addition revealed components above the dominant smooth distribution, including narrow spikes due to tidal streams. Recent hydrodynamical simulations of Milky Way-like galaxies including baryons, which have a non-negligible effect on the DM distribution in the Solar neighbourhood, find velocity distributions that are indeed close to Maxwellian, arguing that the SHM is a good approximation.

Ultimately the goal is to determine the velocity distribution from observations (for example by studying the motion of stars that share the same kinematics as the DM), and the *Gaia* satellite data offers a unique opportunity to study the various stellar populations. Recently it was revealed that the local stellar halo has two components: a quasi-spherical, weakly rotating structure with metal-poor stars, and a flattened, radially anisotropic structure of metal-rich stars, which arose due to accretion of a large ( $10^{11-12} M_\odot$ ) dwarf galaxy around  $(8-10) \times 10^9$  y ago [54]. The expectation is that the local DM halo shows a similar bimodal structure, and first velocity distributions of the two components - using the stellar populations as tracers - were inferred in [55]. In Ref. [56], an updated halo model is introduced: it includes the anisotropic structure seen in the *Gaia* data and provides an analytic expression for the velocity distribution. The value of the local DM density is updated to  $(0.55 \pm 0.17)$  GeV/cm<sup>3</sup>, where the 30% error accounts for the systematics. The circular rotation and the escape speeds are updated to  $v_c = (233 \pm 3)$  km/s and  $v_{esc} = 528^{+24}_{-25}$  km/s. The

former is in agreement with a new Bayesian estimation of the circular velocity using Gaia DR3, of  $v_c = (233 \pm 7)$  km/s [57]. With Gaia DR3, new stellar streams are being discovered, some of these likely originating from the disruption and merger of dwarf galaxies. The study of the velocities of such streams will allow for increasingly improved constraints on both the DM subhalo density profiles and the velocity distributions.

#### 27.4.2 Small-scale challenges

The  $\Lambda$ CDM framework is tremendously successful at explaining the observed large-scale structures of the Universe (corresponding to distances  $\geq 1$  Mpc, the typical inter-galactic distance), as well as the main properties of galaxies that form within DM haloes, see the comprehensive review in Ref. [58]. The observed large-scale structure is consistent with point-like, cold DM particles that interact purely via the gravitational force. However, in the past decades, observations at scales below  $\sim 1$  Mpc, where structure formation becomes strongly nonlinear, turned out more problematic to be described within the  $\Lambda$ CDM model. The main *small-scale challenges* are known as: the missing satellites problem, the cusp-core problem and the too-big-to-fail problem. Initially these issues, which are not all independent of one another, arose by comparing theoretical predictions from dark-matter-only simulations to observation. While their most likely solutions are in dissipative, baryonic physics (such gas cooling, star formation, supernovae feedback), see the recent reviews in Ref. [59, 60], the small-scale problems could in addition call for a modification or an extension of the  $\Lambda$ CDM paradigm. Most importantly, the ever increasing amount of data on the satellites of the MW and M31 are used to constrain alternative DM models.

**The missing satellites problem:** High-resolution cosmological simulations of DM haloes the size of the MW predict hundreds or thousands of subhaloes with masses that are in principle large enough to allow for galaxy formation ( $> 10^7 M_\odot$ ). Yet less than  $\sim 100$  satellite galaxies with masses down to  $\sim 300 M_\odot$  are known to orbit our galaxy within 300 kpc. Galaxies in the field show a similar under-abundance. One solution could be that galaxy formation becomes increasingly inefficient as the halo mass drops, and thus the smallest DM haloes have naturally failed to form galaxies. Progress in both observations and theoretical modeling of observable properties of dwarf galaxies show that there is very scant evidence for a “missing satellite problem” [60]. Nonetheless, additional, related strong tensions remain, including the *diversity of observed rotation curves* [61] and the *unexpected alignment of satellite planes*, the latter issue possibly solved by high-precision simulations tracking inflow along filaments of the cosmic web [62].

**The cusp-core problem:** The mass density profiles of DM haloes in  $\Lambda$ CDM simulations rise steeply at small radii,  $\rho(r) \propto r^{-\gamma}$ , with  $\gamma \simeq 0.8 - 1.4$ . This is in contrast to the observed density profiles of many low-mass galaxies (albeit not all), the rotation curves of which are best fit with constant-density cores,  $\gamma \simeq 0 - 0.5$ . A related issue is that simulations predict more DM than measured in the central regions of galaxies (also known as the central density problem). A likely solution is that baryonic feedback modifies the structure of DM haloes. Hydrodynamic simulations which include the effects of baryons on galaxy formation have shown that baryonic feedback (e.g., supernova-driven blowouts) can erase the central cusps and produce core-like density profiles. Surveys of satellites of hundreds of galaxies similar to the Milky Way, such as SAGA [63], will likely provide important observational information.

**The too-big-to-fail problem:** This problem is related to the fact that the dark matter halos of the largest observed Milky Way satellites are typically much smaller than those of the most massive subhalos of simulated Milky Way-like halos. DM haloes of such masses are thought to be too massive to have failed to form stars (hence the name of the problem), especially if lower-mass subhaloes are capable of doing so. A similar issue is present in Andromeda and in field galaxies outside the Local Group. Possible solutions include lowering the mass assumed for the

Milky Way host halo, or baryonic effects including tidal stripping and larger-than-expected inner cores [60]. Other issues relate to the origin of ultra-faint galaxies, and the opposite problem of dwarf galaxies with very little dark matter given their stellar mass; there exist proposed solutions to both challenges, including the “bullet dwarf” scenario of Ref. [64].

The solutions that were briefly mentioned above do not require modifications to the  $\Lambda$ CDM framework. Other solutions involve either modifications of linear theory predictions (via the nature of the DM particle, e.g., Warm DM - WDM) or modifications of nonlinear predictions (via DM models that involve a self-interaction of DM particles - SIDM). WDM models postulate particles with masses at the keV-scale, and the observed number of dark-matter-dominated satellites is used to set a lower limit on the number of subhaloes in the MW and thus a lower limit on the particle’s mass [59]. Current constraints are in the range  $m_{WDM} > (1.6 - 2.3)$  keV. Cosmological simulations with SIDM find that  $\sigma/m_{SIDM} \simeq (0.5-10)$  cm<sup>2</sup>/g can alleviate the cusp-core and too-big-to-fail problems, giving rise to DM cores in dwarf galaxies with sizes of (0.3-1.5) kpc [13]. Galaxy clusters provide important constraints, and their large central DM densities prefer models with  $\sigma/m_{DM} \lesssim 0.1$  cm<sup>2</sup>/g [65]. Thus, if SIDM is to solve the small-scale CDM problems and obey the constraints observed on the scales of clusters,  $\sigma$  must depend on the velocity of the particle: it must increase as the rms speed of the particle decreases from the scale of clusters ( $v \sim 10^3$  km/s) to the scale of dwarf galaxies ( $v \sim 10$  km/s).

## 27.5 Dark matter models

Particle DM model building is deeply intertwined with the question of the nature of physics beyond the Standard Model (BSM) of particle physics<sup>1</sup>. Directions in this area have followed a few strategies, including, but not limited to

(1) pursuing DM candidates embedded in frameworks that include solutions to other open issues in particle physics, for example WIMPs in connection with electroweak-scale new physics that addresses the hierarchy problem, such as supersymmetry (see the Supersymmetry reviews Sec. 88 and 88); axions in connection with frameworks that address the strong  $CP$  problem (see Axions and Other Similar Particles—Sec. 90); sterile neutrinos in connection with the problem of neutrino masses and mixing (see the Neutrino Masses, Mixing, and Oscillations—Sec. 14); or (2) *ad hoc*, or *bottom-up* models built with the intent of addressing or explaining a putative experimental (e.g. particle physical anomalies) or observational (e.g. astronomical) signal.

**WIMPs:** The WIMP paradigm has been a preferred framework chiefly because it often arises in beyond the Standard Model scenarios that address the hierarchy problem whilst also providing a simple mechanism to explain the observed relic abundance via the “WIMP miracle” described above. Perhaps the most notable example of a framework containing a paradigmatic WIMP is the minimal supersymmetric extension to the Standard Model, if the lightest supersymmetric particle is a neutralino (the mass eigenstate resulting from the mixing of the supersymmetric partners to the Higgses and to the SU(2) and hypercharge gauge bosons, and, possibly, of additional singlet scalars); purely SU(2) sneutrinos have long been ruled out by direct detection, but with suitable mixing with “inert” (gauge-singlet) sneutrinos they can also play the role of WIMP candidates. For more details see the the Supersymmetry—Sec. 88 and 89 in this *Review*. Other non-supersymmetric WIMP models include models with a Higgs or  $Z$  (or  $Z'$ ) portal, universal extra dimensions [32], and other models with extra (warped or flat) dimensions, little Higgs theories, technicolor and composite Higgs theories, among others (see e.g. the review in [66]).

**Axions and axion-like particles:** Axions are an especially compelling example of a broad category of DM candidates encompassing very light scalar or pseudoscalar fields. The QCD axion provides a solution to the strong  $CP$  problem, and is at present a viable DM candidate (see Sec. 90

<sup>1</sup>Notice that this includes the case of PBHs, as successful formation of the correct number density of PBHs involves new ingredients beyond standard cosmology and particle physics

for details on motivations, production mechanisms, and detection prospects for the QCD axion). Ultra-light, bosonic DM generally implies the imprint of quantum effects on macroscopic scales (hence the name of *wave* or *fuzzy* DM). Specifically, some of the small-scale issues mentioned in sec. 27.4 can be addressed if the de Broglie wavelength of the DM, of mass  $m_a$  and velocity  $v_a$ ,

$$\frac{\lambda}{2\pi} = \frac{\hbar}{m_a v_a} \simeq 1.9 \text{ kpc} \left( \frac{10^{-22} \text{ eV}}{m_a} \right) \left( \frac{10 \text{ km/s}}{v_a} \right) \quad (27.7)$$

is comparable to the size of the smallest observed gravitationally collapsed structures, roughly, for a self-gravitating system of mass  $M$ , a scale  $r \simeq GM/v^2$ . The typical expectation is the formation of a soliton-like core in the DM density profile of size  $\lambda$ , thus inversely proportional to the DM mass, with an upper limit on the central density of around

$$\rho_s \lesssim 7 M_\odot/\text{pc}^3 \left( \frac{m_a}{10^{-22} \text{ eV}} \right)^6 \left( \frac{M}{10^9 M_\odot} \right) \quad (27.8)$$

for a halo of virial mass  $M$ . Additionally, wave DM predicts that halos lighter than around  $10^7 (m_a/10^{-22} \text{ eV})^{-3/2} M_\odot$  should not exist [67], and that the number of halos in the local universe with a mass at or less  $10^9 (m_a/10^{-22} \text{ eV})^{-4/3} M_\odot$  [68] be significantly depleted, addressing in part the too big to fail and missing satellite problems (see Sec. 27.4 above). Light bosonic DM is necessarily produced non-thermally [69], and the connection with the visible sector need not, but might, exist.

**Dark photons:** Light *vector* bosons such as a “dark photon”  $V$  with a mass below  $m_V < 2m_e$ , can be cosmologically stable (depending upon its kinetic mixing coupling with the visible photon) and be a viable DM candidate. Light dark photons can be produced in the early universe through scattering or annihilation via processes such as  $\gamma e^\pm \rightarrow V e^\pm$  or  $e^+ e^- \rightarrow V \gamma$ , or via resonant photon-dark photon conversion, or from a condensate seeded by inflationary perturbations [70], or from a misalignment mechanism similar to the one commonly invoked for axion production; constraints on the parameter space stem from a combination of direct detection experiments, where the dark photon is absorbed and leads to a large ionization signal, from stellar cooling constraints from the Sun, horizontal branch stars, and red giants, and from CMB and the diffuse radiation from the  $V \rightarrow 3\gamma$  decay mode. More broadly, light dark (pseudo-)scalars and vectors can be best constrained with experiments that rely on their wave-like behaviour and/or on their possible “portal” with the visible sector. A broad assortment of experiments is sensitive to the range of masses between  $10^{-22}$  eV and  $10^{-2}$  eV. Among these experimental efforts, the lowest masses are probed by torsion balance experiments [71, 72], atom interferometry [73], comagnetometers [74, 75], and even gravitational wave detectors [76]; at increasing masses, if the light bosons couple electromagnetically, they can generate effective currents which are detectable with different apparatus depending on the relevant, mass-dependent target frequency. The experimental portfolio includes the broadband axion search ABRACADABRA [77, 78], the LC resonator DM Radio [79], lumped-element LC resonators [80], and cavity resonators such as HAYSTAC [81] and ADMX [82].

**Sterile Neutrinos:** Sterile (gauge-singlet) neutrinos, assumed to share a Dirac mass term with ordinary,  $SU(2)_L$ -active neutrinos, have long been considered viable DM candidates [83]. The mostly-stable mass eigenstate participates in  $SU(2)_L$  interactions via a mixing parameter  $\theta \ll 1$  that controls much of the particle’s phenomenology. In particular, the sterile neutrino possesses an inverse-lifetime on the order of  $\tau^{-1} \sim G_F^2 m_\nu^5 \theta^2$ , forcing the mixing to not exceed

$$\theta < 3.3 \times 10^{-4} \left( \frac{10 \text{ keV}}{m_\nu} \right)^5 \quad (27.9)$$

in order for the lifetime to exceed the age of the universe. While the main decay channel is to three active neutrinos, observationally the radiative decay mode to one neutrino plus a photon is much more relevant, giving rise to a quasi-monochromatic photon line at half the sterile neutrino mass. A recent tentative signal at 3.5 keV was reported from stacked observations of clusters of galaxies, individual clusters [84, 85], and the Galactic center [86] with both the XMM and Chandra X-ray observatories. The signal however was not detected in a large sample of galaxies and groups of galaxies [87] and dwarf galaxies [88], and especially Draco [89], shedding strong doubts on its sterile neutrino decay origin. Future observations with increased energy resolution might conclusively pinpoint the origin of the 3.5 keV emission [90].

**Models with rich dark sectors:** The absence of any conclusive signals from DM as a particle thus far motivates the hypothesis that the DM be charged under some new “hidden” dark-sector force, an idea that dates back many decades [91], including in the guise of “mirror DM” (more recently in the context of “neutral naturalness”). Top-down motivation for hidden-sector DM comes from string theory [92], although TeV-scale BSM framework such as supersymmetry and composite Higgs models can also naturally accommodate hidden sectors [93]. Although no coupling of the visible sector to the hidden sector need exist in principle, there are a few reasons to expect it [94]. The mass scale for hidden-sector DM is broader than, but overlapping with, that for WIMPs (this latter being limited to roughly between a few GeV and a few TeV). In particular, while some motivation exists for electroweak-scale hidden sectors, light, sub-GeV hidden sectors have a strong theoretical underpinning, and offer novel detection avenues and opportunities. The phenomenology of hidden-sector DM depends primarily on the nature of the force and its force carrier. The most-widely considered cases are (pseudo-)scalar and (axial-)vector mediators. Among the structures for the mediators’ coupling to the visible sector, renormalizable “portals” include the  $H^\dagger H$  operator, through Lagrangian terms of the type  $(\mu\phi + \lambda\phi^2)H^\dagger H$ , coupling to the hypercharge field strength  $B^{\mu\nu}$  via kinetic mixing,  $\epsilon' B_{\mu\nu}F'^{\mu\nu}$ , and the “neutrino” portal,  $y_n LHN$ , where  $L$  is the lepton doublet of any generation,  $N$  is a right-handed neutrino,  $H$  is the SM Higgs doublet, and  $y_n$  the Yukawa coupling. Other possibilities are for instance a vector mediator directly coupled to SM fermions charged under its corresponding symmetry [95], or a  $Z'$  associated to  $U(1)_{B-L}$ . Additional possibilities, arising for instance from vector couplings to anomalous global symmetries of the SM like baryon or lepton number, also exist [94]. The accelerator program necessary to probe hidden-sector DM often involves small-scale colliders and fixed-target experiments, with experiments utilizing missing energy and momentum offering the best sensitivity. Beam-dump experiments can test large ranges of DM-mediator couplings as long as mediators decay or scatter inside the detector (see e.g. the recent review [96]). Such experiments can also probe dark sectors with light vectors coupled to visible matter besides gauge kinetic mixing: an instance are neutrino trident scattering used to place bounds on e.g.  $L_\mu - L_\tau$   $Z'$  gauge bosons. Being virtually unconstrained, the phenomenology of dark sectors can be arbitrarily rich, with possibilities ranging from dark non-Abelian gauge interactions creating non-trivial self-interacting and/or particle number-changing dynamics, to models of “dynamical” DM, with multi-component, unstable DM candidates and a time-variable effective total DM abundance and equation of state [97].

## 27.6 Laboratory detection of dark matter

Laboratory searches for DM particles can be roughly classified in direct detection experiments, axion searches (see Axions and Other Similar Particles—Sec. 90), and searches at accelerators and colliders.

### 27.6.1 Searches at Accelerators and Colliders

Various searches for dark matter have been carried out by the CMS and ATLAS collaborations at the LHC in  $pp$  collisions [98–102]. In general, these assume that dark matter particles escape

the detector without interacting leading to significant amounts of missing energy and momentum.

Searches for DM with the LHC and other colliders have targeted DM models that interact with the SM via Higgs or  $Z$  boson exchange, effective field theories with heavy mediators, UV-complete models such as supersymmetry, models with long-lived particles, and models with rich dark sectors. The experimental program correspondingly includes searches for invisible-particle production mediated by a SM boson, generic searches for invisible particles produced via new particle mediators, and specific searches for complete models.

There are a variety of types of signals for DM, as noted by Ref. [98]:

(a) the imbalance in the transverse momentum in an event due to the presence of DM particles, produced together with one Standard Model particle,

(b) a bump in the di-jet or di-lepton invariant mass distributions, or

(c) an excess of events in the di-jet angular distribution, produced by a dark matter mediator.

No signal for DM has been observed in the LHC experiments so far. Instead, limits are set on masses, couplings, and cross-sections. The latter can be compared, generally in a model-dependent way, with direct detection experiments.

Searches strategies are designed to optimize signal-to-noise by selecting search-specific cuts: a model-independent instance is initial-state electromagnetic or strong-interaction radiation plus missing transverse energy. Collider searches for DM inform, and are informed, by DM searches through direct or indirect detection (see below), and, if possible, by the inferred thermal relic DM abundance. The collider searches alone cannot prove that a discovery is of dark matter.

In the latter category, searches for DM with the LHC and other colliders have targeted DM models that interact with the SM via Higgs or  $Z$  boson exchange, effective field theories with heavy mediators, UV-complete models such as supersymmetry, models with long-lived particles, and models with rich dark sectors. The experimental program correspondingly includes searches for invisible-particle production mediated by a SM boson, generic searches for invisible particles produced via new particle mediators, and specific searches for complete models. Searches strategies are designed to optimize signal-to-noise by selecting specific search-specific cuts: a model-independent instance is initial-state electromagnetic or strong-interaction radiation plus missing transverse energy.

New fixed-target experiments are increasingly probing lighter, sub-GeV dark sectors; thermal, or quasi-thermal relics (such as asymmetric, SIMP, ELDER DM models) provide sharp, largely model-independent experimental targets in the case of direct annihilation to Standard Model particles; even “secluded” annihilation to dark-sector particles can be probed with fixed-target experiments, albeit with some model-dependent caveats. Accelerator searches provide unique ways to test light DM models in that they present a lower dependence on the DM particle nature, that could e.g. drive suppressed velocity-dependent direct detection cross sections, and on kinematic thresholds that can similarly suppress rates with other search strategies; additionally, accelerator searches offer opportunities to explore dark sectors in greater detail than other search strategies [94].

Experimental approaches to explore scenarios with a light DM  $\chi$  and mediator  $A'$  include (i) searches for missing mass in exclusive reactions such as  $e^+e^- \rightarrow \gamma(A'\chi\bar{\chi})$  or  $e^-p \rightarrow e^-p(A'\chi\bar{\chi})$ , (ii) missing momentum/energy, e.g. in fixed-target reactions such as  $eZ \rightarrow eZ(A'\chi\bar{\chi})$ , (iii) electron and proton beam dump, where the DM particle is detected from scattering in a downstream detector after being produced in the beam dump, (iv) direct dark photon searches, when the mediator cannot decay to the dark matter,  $m_{A'} < 2m_\chi$ . Current facilities actively probing the methods listed above include APEX and HPS and JLab, MiniBooNE at Fermilab, NA64 at CERN, and TREK at J-PARC. Future experiments that will eventually contribute to covering the mentioned thermal targets include Belle-II at KEK, MAGIX at MESA, PADME at LNF, SHIP at CERN, VEPP3 at BINP, BDX at JLab, COHERENT at ORNL, DarkLight at JLab, LDMX at SLAC or

JLab, MMAPS at Cornell, SBN at Fermilab, and SeaQuest [94].

### 27.6.2 Direct detection formalism

Direct detection experiments mostly aim to observe elastic or inelastic scatters of Galactic DM particles with atomic nuclei, or with electrons in the detector material. Predicted event rates assume a certain mass and scattering cross section, as well as a set of astrophysical parameters: the local density  $\rho_0$ , the velocity distribution  $f(\vec{v})$ , and the escape velocity  $v_{esc}$  (see Sec. 27.4).

**Table 27.1:** Best constraints from direct detection experiments on the SI (at high  $>5$  GeV and low  $< 5$  GeV masses) and SD DM-nucleon couplings.

Experiment	Target	Fiducial mass [kg]	Cross section [cm <sup>2</sup> ]	DM mass [GeV]	Ref.
<b>Spin independent high mass (<math>&gt;5</math> GeV)</b>					
LUX-ZEPLIN	Xe	5500	$9.2 \times 10^{-48}$	36	[103]
PandaX-4T	Xe	2670	$3.8 \times 10^{-47}$	40	[104]
XENONnT	Xe	4180	$2.6 \times 10^{-47}$	30	[105]
SuperCDMS	Ge	12	$1.0 \times 10^{-44}$	46	[106]
DarkSide-50	Ar	20	$1.9 \times 10^{-43}$	10	[107]
DEAP-3600	Ar	2000	$3.9 \times 10^{-45}$	100	[108]
<b>Spin independent low mass (<math>&lt; 5</math> GeV)</b>					
LUX (Migdal)	Xe	118	$6.9 \times 10^{-38}$	2	[109]
XENON1T (Migdal)	Xe	1042	$3 \times 10^{-40}$	2	[110]
XENON1T (ionisation only)	Xe	1042	$3.6 \times 10^{-41}$	3	[111]
DarkSide-50 (ionisation only)	Ar	20	$1.4 \times 10^{-42}$	2	[107]
SuperCDMS (CDMSlite)	Ge	0.6	$2 \times 10^{-40}$	2	[112]
SuperCDMS (CDMSlite, Migdal)	Ge	0.6	$6 \times 10^{-38}$	2	[113]
CRESST	CaWO <sub>4</sub> - O	0.024	$1 \times 10^{-39}$	2	[114]
CRESST	Si	0.0035	$4.5 \times 10^{-32}$	0.15	[115]
DAMIC	Si	0.3	$1 \times 10^{-40}$	4	[116]
NEWS-G	Ne	0.3	$1 \times 10^{-38}$	2	[117]
<b>Spin dependent proton</b>					
PICO60	C <sub>3</sub> F <sub>8</sub> - F	49	$3.2 \times 10^{-41}$	25	[118]
PandaX-4T	Xe	2670	$1.7 \times 10^{-40}$	40	[119]
LUX-ZEPLIN	Xe	5500	$4.2 \times 10^{-41}$	32	[103]
XENONnT	Xe	4180	$1.4 \times 10^{-40}$	30	[105]
<b>Spin dependent neutron</b>					
PandaX-4T	Xe	2670	$5.8 \times 10^{-42}$	40	[119]
LUX-ZEPLIN	Xe	5500	$1.5 \times 10^{-42}$	30	[103]
XENONnT	Xe	4180	$4.3 \times 10^{-42}$	30	[105]

**Interactions with atomic nuclei:** For DM scattering off nuclei, the differential scattering rate  $R$  as a function of nuclear recoil energy  $E_R$  is

$$\frac{dR(E_R, t)}{dE_R} = N_T \frac{\rho_0}{m_{\text{DM}}} \int_{v > v_{min}} v f(\vec{v} + \vec{v}_E(t)) \frac{d\sigma(E_R, v)}{dE_R} d^3 v, \quad (27.10)$$

where  $N_T$  is the number of target nuclei,  $m_{\text{DM}}$  is the mass of the DM particles,  $v = |\vec{v}|$  is the speed of the particle in the experiment's rest frame,  $f(\vec{v} + \vec{v}_E(t))$  is the velocity distribution in the Earth's frame,  $v_{min}$  is the minimum speed of the DM particles that can cause a recoil energy  $E_R$  and  $\sigma$  is the scattering cross section on the nucleus [29, 120]. For elastic scattering, the minimum velocity is  $v_{min} = (m_N E_R / 2m_r^2)^{1/2}$ , with  $m_N$  being the mass of the nucleus, and  $m_r = (m_N m_{\text{DM}}) / (m_N + m_{\text{DM}})$  the reduced mass of the nucleus-DM system. In case of inelastic scattering, the minimum

speed becomes  $v_{min} = (m_N E_R / 2m_r^2)^{1/2} + E^* / (2m_N E_R)^{1/2}$ , with the nuclear excitation energy  $E^*$ , for part of the kinetic energy of the incoming particle will be spent on exciting the nucleus. The prompt de-excitation energy, if observed in addition to the nuclear recoil energy, will boost the region-of-interest to higher energies [121].

If one assumes the standard, leading order spin-independent (SI) and spin-dependent (SD) interactions, which couple to the charge/mass and spin of the nucleus, respectively, the differential cross-section is proportional to the inverse squared speed of the DM particle,  $d\sigma/dE_R \propto v^{-2}$ , and the dependence on the velocity distribution can be expressed as:

$$g(v_{min}, t) = \int_{v > v_{min}} \frac{f(\vec{v} + \vec{v}_E(t))}{v} d^3v. \quad (27.11)$$

This functions allows for the comparison of various experimental results independently of the underlying velocity distribution [122], for a given DM mass. The time-integrated differential cross section is the sum of the SI and SD contributions:

$$\frac{d\sigma(E_R, v)}{dE_R} = \frac{m_N}{2m_r^2 v^2} \left( \sigma_0^{SI} F_{SI}^2(E_R) + \sigma_0^{SD} F_{SD}^2(E_R) \right), \quad (27.12)$$

where  $F^2(E_R)$  are the nuclear form factors and  $\sigma_0$  the cross-sections in the limit of zero momentum transfer. Since the incoming particle velocity is  $v/c \sim 10^{-3}$ , the nuclear recoil energy is at most tens of keV (much smaller than typical nuclear binding energies per nucleon), and the momentum transfer  $q = (2m_N E_R)^{1/2} \sim \mathcal{O}(10 - 100)$  MeV. This implies that  $1/q$  can be of the same order as nuclear radii  $R \sim A^{1/3}$  fm, and that nuclei are not point-like from the perspective of a DM particle. The cross sections will thus involve nuclear form factors. These were calculated in [123] and [124] for the SI and SD case, respectively, for specific target nuclei, while the cross sections are often expressed in terms of single-nucleon cross sections and effective couplings of the DM particle to protons and neutrons. In the SI case, all the nucleons in the nucleus contribute coherently to the cross-section (under the assumption of isospin independence in the DM couplings). Dominant sources of uncertainty are the nucleon sigma terms, especially for Higgs-dominated interactions, where the couplings are proportional to the quark masses. An overview is presented in Ref. [125]. For SD scattering, the nuclear spin contents due to the protons and neutrons must be considered.

The interactions of DM particles with nuclei can be treated in a non-relativistic effective field theory (NR-EFT) approach, which considers more general DM scenarios based on the lowest-order, four-field operators that describe the couplings to nucleons. These operators, which correspond to different types of interactions between the DM and quark fields, can be momentum- and velocity-dependent, and might be leading when momentum-independent interactions are suppressed, or even vanish in the limit of zero momentum [126, 127]. In Ref. [127, 128] all 15 operators (arising from 20 possible bilinear combinations between the DM and nucleon fields) which obey Galilean-invariance,  $T$ -symmetry and are Hermitian are written out up to quadratic order in  $q$ , and the nuclear response functions evaluated in shell-model calculations for DM targets made of F, Na, Ge, I and Xe isotopes. The connection to particle physics within the context of *simplified DM models* is made in Ref. [129, 130], where the simplified models assume a single DM particle with one mediator which couples it to quarks. More recently the DM-nucleus scattering was also analysed in the framework of chiral effective field theory (Ch-EFT), a low-energy effective theory of QCD, which allows for a consistent derivation of the nuclear responses beyond the leading-order expressions [131, 132]. Ch-EFT preserves the QCD symmetries, and predicts DM couplings to two nucleons (e.g., when the hypothetical particle couples to a virtual pion exchanged between the nucleons). It also provides a power counting that suggests a hierarchy of the various NR-EFT operators, which is

however approximate given that the couplings between the DM and the Standard Model fields are not known. The generalized SI structure factors for spin-1/2 and spin-0 DM particles and various isotopes of F, Si, Ar, Ge and Xe employed in direct detection experiments are provided in Ref. [132].

**Scattering off bound electrons and absorption:** For DM particle masses below the GeV-scale, most searches for DM-nucleus scattering rapidly lose sensitivity, due to energy thresholds around a few 100 eV - few keV. As an example, a light DM particle with a mass of 100 MeV and  $v \propto 10^{-3}c$  will induce a nuclear recoil energy of about 0.5 eV in a target made of argon. Another strategy is to search for DM scattering off bound electrons, allowing for all of the kinetic energy (50 eV in the above case) to be transferred to the material [133]. The leading possibilities are ionisation, excitation, and molecular dissociation processes, which typically require energies of (1-10) eV, and thus allow to probe scattering of DM particles with masses down to the  $\mathcal{O}(\text{MeV})$  range.

For a bound electron with binding energy  $E_B$  DM particle masses of  $m_{\text{DM}} \geq 250 \text{ keV} \times E_B / 1 \text{ eV}$  can in principle be probed. The signal depends on the material, and can consist of one or more electrons (in semiconductors, noble liquids, graphene), one or more photons (in scintillators) or phonons (in superconductors and superfluids) and quasiparticles (in superconductors). As an example, the differential event rate for ionization in atoms is given by:

$$\frac{dR_{ion}}{d \ln E_R} = N_T \frac{\rho_0}{m_{\text{DM}}} \frac{d\langle\sigma_{ion}v\rangle}{d \ln E_R}, \quad (27.13)$$

where  $E_R$  is the recoil energy transferred to the electron,  $\langle\sigma_{ion}v\rangle$  is the thermally averaged ionization cross section and  $N_T$  is the number of target atoms per unit mass. The cross-section is related to the non relativistic DM-electron elastic scattering cross-section ( $\sigma_e$ ):

$$\frac{dR_{ion}}{d \ln E_R} = \frac{6.2}{A} \left( \frac{\rho_0}{0.4 \text{ GeV cm}^{-3}} \right) \left( \frac{\sigma_e}{10^{-40} \text{ cm}^2} \right) \left( \frac{10 \text{ MeV}}{m_{\text{DM}}} \right) \times \frac{d\langle\sigma_{ion}v\rangle/d \ln E_R}{10^{-3}\sigma_e} \frac{\text{events}}{\text{kg d}} \quad (27.14)$$

Predicted differential rates in various materials (He, Ar, Ge, Xe) and for different particle masses are shown in [133], together with cross section sensitivities as a function of mass and expected background rates from neutrinos. More recently, rates of electronic transitions induced by DM-electron scattering on Xe, Si and Ge for spin 0, spin 1/2, and spin 1 DM models were calculated in [134]. The code **EXCEED-DM** (extended calculation of electronic excitations for direct detection of dark matter) can compute DM-electron interaction rates with inputs from a variety of *ab initio* electronic structure calculations [135].

Two classes of DM candidates, axion-like-particles (ALPs) and dark (or hidden) photons (see Sec. 27.5), can be absorbed in a target material by interactions with bound electrons via the axioelectric effect, which is analogous to the photoelectric effect: a boson is absorbed by a bound electron, which is then ejected from the atom [70, 136, 137]. The dark photon arises in extensions of the SM by a new massive or massless U(1)' field, coupled to the SM U(1)<sub>Y</sub> via a kinetic mixing term  $\kappa$ , see Sec. 27.5. The absorption cross-section of a massive, NR particle  $m_V$  with coupling  $e' = e\kappa$  to electrons is (in natural units, and for energies  $E_V \ll m_e$ )

$$\sigma_{abs} = \frac{\alpha'}{\alpha} \left( \frac{E_V}{2m_e} \right)^2 \sigma_{pe}, \quad (27.15)$$

where  $\sigma_{pe}$  is the photoelectric cross-section, and an analogue to the electromagnetic fine structure constant  $\alpha$  is introduced,  $\alpha' = (e\kappa)^2/4\pi$ . The rate per atom is

$$R \simeq \frac{\rho_0}{m_V} \times \kappa^2 \sigma_{pe}. \quad (27.16)$$

Since the kinetic energy of the dark photon is negligible compared to its rest energy, a mono-energetic peak at its mass is expected in the spectrum of a direct detection experiment. Dark photons with a thermally generated abundance are excluded by direct detection experiments [70], however non-thermal mechanisms (e.g., via perturbations during inflation) could create the relic abundance, see Section 27.3.

Similarly to axions, ALPs arise in the spontaneous breaking of a global symmetry, and are phenomenologically described by a mass  $m_a$  and a decay constant  $f_a$ . Unlike for QCD axions, however, there is no strict relation between  $m_a$  and  $f_a$ . The coupling strength to electrons with mass  $m_e$  is parameterised by  $g_{ae} = 2m_e/f_a$ , and the absorption cross section of a particle with incoming velocity  $v_a$  is related to the cross-section for the photoelectric effect as

$$\sigma_{abs}v_a \simeq \frac{3E_a^2}{4\pi\alpha f_a^2}\sigma_{pe} = \frac{3g_{ae}^2}{4\pi\alpha} \left(\frac{E_a}{2m_e}\right)^2 \sigma_{pe}. \quad (27.17)$$

As in the case of the dark photon, the signature is a mono-energetic peak at the mass of the particle, broadened by the energy resolution of the detector. Constraints on the couplings of ALPs and dark photons to electrons from direct detection experiments in  $m_a$  and  $m_V$  mass ranges from  $\sim (1 - 10^4)$  eV were derived in Ref. [138, 139], and compared to indirect limits from anomalous energy losses in the Sun, in red-giant and horizontal-branch stars. For a detailed discussion of axion and ALP searches, we refer to the *Axion* review.

### 27.6.3 Current and future direct detection technologies

Direct detection experiments aim to observe the small (keV-scale and below) and rare (fewer than  $\sim 1$  event/(kg y)) signals which are induced by DM particle scatters in a detector, mostly in the form of ionisation, scintillation or lattice vibrations. A majority of experiments detects more than one signal, which allows to distinguish between scattering off of electrons (electronic recoils, ER) and off of atomic nuclei (nuclear recoils, NR). A 3D position resolution is required to define central detector regions (or fiducial volumes) with low background rates from surrounding materials, and the distinction between single- versus multiple-scatters rejects a significant fraction of backgrounds, given that DM will scatter at most once. We refer to [140, 141] for recent reviews of the field.

**Specific signatures:** For NRs, the shape of the differential recoil spectrum is exponentially falling with recoil energy, and depends on the mass of the particle and on the nuclear mass. Unless  $m_{DM} \gg m_N$ ,  $m_{DM}$  can in principle be determined from the measured recoil spectrum, where multiple targets will provide tighter constraints [142]. The Earth's motion through the MW induces a seasonal variation of the total event rate and a forward-backward asymmetry in a directional signal [143, 144]. The annual modulation is due to the Earth's motion in the Galactic rest frame, which is a superposition of the Earth's rotation around the Sun and the Sun's rotation around the Galactic center. Since the Earth's orbital speed is much smaller than the Sun's speed, the expected amplitude of the modulation is  $\simeq 5\%$ . In the SHM, the period is one year, and the phase is 150 d (June 2), when both speeds add up maximally. This expectation is modified for different DM distributions, e.g. in the case of sub-structures such as clumps and streams [145, 146] and a DM disc [147]. In addition, the modulation changes phase at a specific recoil energy (known as crossing-energy) [148], which depends on the DM and nuclear mass, allowing to in principle determine  $m_{DM}$  if low energy thresholds can be achieved. A powerful signature is provided by the ability to detect the axis and direction of the recoiling nucleus. Since the DM flux in the laboratory frame is peaked in the direction of motion of the Sun towards the constellation Cygnus, the recoil spectrum is peaked in the opposite direction. The observation of such a dipole feature would provide a 'smoking-gun' evidence for DM, where the forward-backward rates can differ by a factor of  $\sim 10$ , depending on the energy threshold. Ref. [149] provides a review of the theoretical framework and of the discovery reach of directional detectors.

**Backgrounds, including neutrinos:** Early direct detection experiments employing low-background Ge spectrometers featured background levels around 2 events/(kg d keV), while the latest generation of liquid Xe experiments reduced this noise by almost five orders of magnitude, to  $4 \times 10^{-5}$  events/(kg d keV). In liquid xenon detectors, the measured ER spectra at low energies are for the first time dominated by solar  $pp$  neutrino interactions, second-order weak decays, as well as  $^{214}\text{Pb}$   $\beta$ -decays from radon mixed with the xenon. Other backgrounds are due to the radioactivity of detector components, followed by cosmic muons and their secondaries such as fast neutrons. The cosmic and environmental radiation are suppressed by going deep underground and surrounding the experiments with appropriate shielding structures (mainly large water Cherenkov detectors for the current and next-generation detectors). Activation of materials via cosmic-ray interactions produce long-lived radio-nuclides (e.g.,  $^{39}\text{Ar}$ ,  $^{60}\text{Co}$ ,  $^{68}\text{Ge}$ ,  $^{32}\text{Si}$ , etc), while long-lived, human-made isotopes ( $^{85}\text{Kr}$ ,  $^{137}\text{Cs}$ , etc) can mix with detector materials or generate surface backgrounds. For details, we refer to *Section 36.6* of this *Review*.

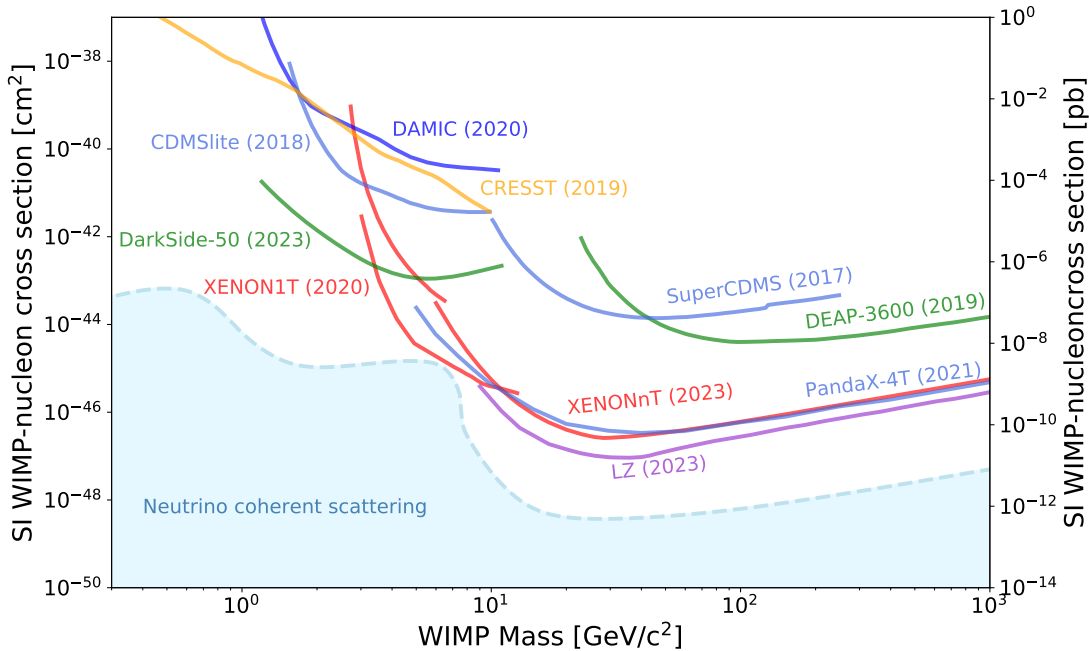


**Figure 27.1:** Upper limits on the SI DM-nucleon cross section as a function of DM mass.

The final backgrounds are due to the irreducible neutrino flux from the Sun, the atmosphere and the diffuse supernovae background [150]. Solar  $pp$ -neutrinos start dominating the electronic recoil background due to elastic neutrino-electron scatters, at a level of  $\sim (10 - 25)$  events/(t y) below energies of  $\sim 100$  keV, while coherent elastic neutrino-nucleus scatters (CE $\nu$ NS) from  $^8\text{B}$  solar neutrinos will induce up to  $\sim 10^3$  events/(t y) for high-A targets, at nuclear recoil energies below  $\sim$ few keV. Nuclear recoils from atmospheric neutrinos and the diffuse supernovae neutrino background will yield event rates in the range  $(1 - 5)$  events/(100 t y), depending on the detector material. In general,  $^8\text{B}$  and atmospheric neutrinos will impact light ( $\leq 6$  GeV) and heavy (100 GeV and above) DM searches for cross sections on nucleons below  $\sim 10^{-45}$  cm $^2$  and  $\sim 10^{-49}$  cm $^2$ , respectively. The precise cross-sections where neutrinos constitute a dominant background strongly depend on the systematic uncertainties on the neutrino flux normalisation for each source [151]. For very low energy thresholds to nuclear recoils, e.g. 10-30 eV in Ge and Si detectors, CE $\nu$ NS due to the  $^7\text{Be}$  neutrino flux become relevant for exposures of  $\sim 50$  kg y [152]. For DM searches with electron re-

coils via DM-electron scattering and dark photon or ALP absorption, solar neutrinos will also limit the sensitivity to DM masses in the range  $\sim(1\text{-}10^3)$  MeV and  $\sim(1\text{-}10^3)$  eV, respectively, for large exposures  $\sim 1\text{ t y}$ , as shown in Ref. [153].

**Solid-state cryogenic detectors:** Current experiments using the bolometric technique (see *Section 36.5* of this *Review*), together with either charge or light readout, are SuperCDMS (Si, Ge) at Soudan (until 2015) and SNOLAB (in construction), EDELWEISS (Ge) at the Laboratoire Souterrain de Modane (LSM) and CRESST ( $\text{CaWO}_4$ ,  $\text{Al}_2\text{O}_3$ , Si,  $\text{LiAlO}_2$ ) at the Laboratori Nazionali del Gran Sasso (LNGS). These experiments are optimised for low-mass DM searches, and can probe WIMP masses down to  $\sim 0.03$  GeV. CRESST operated a 0.35-g thin wafer Si detector and reached a 10-eV energy threshold, probing DM masses in the range (115–500) MeV, improving existing limits by up to a factor 20 for masses below 160 MeV. CDMSlite operated detectors at higher bias voltages to amplify the phonon signals produced by drifting charges and thus have access to light DM around 1.5 GeV. A reanalysis of the CDMSlite data using the Migdal effect allowed to exclude new parameter space for WIMP-nucleon cross-sections down to 30 MeV [113]. The goal at SNOLAB is to probe the (0.05–5) GeV region down to cross sections of  $\sim 10^{-44}\text{ cm}^2$ . Much smaller, gram-scale versions of cryogenic detectors can have single-charge resolution and thus probe low-mass DM via inelastic electron recoils. A SuperCDMS single-charge sensitive Si detector placed upper limits on DM interacting with electrons for masses between  $(0.5\text{-}10^4)$  MeV, as well as on dark photon kinetic mixing for dark photon masses in the range (1.5–40) eV. With Ge crystals operated at Soudan, SuperCDMS constrained dark photons and ALPs in the mass range 40 eV to 500 keV.

Germanium ionisation detectors operated at 77 K can reach sub-keV energy thresholds and low backgrounds, but lack the ability to distinguish electronic from nuclear recoils. The CDEX-10 experiment at the China Jinping Underground Laboratory (CJPL) uses p-type, point-contact Ge detectors operated in liquid nitrogen to probe DM masses down to 3 GeV. It also reported constraints on the kinetic mixing of dark photons in the mass range (0.1–4.0) keV. The  $0\nu\beta\beta$ -decay experiments Majorana Demonstrator and GERDA have obtained constraints on the couplings of ALPs and dark photons to electrons, with masses between (6–100) keV and (60–1000) keV, respectively. The Majorana Demonstrator improved laboratory constraints on solar axion masses between (1.2–100) eV, setting limits on the axion-photons coupling of  $g_{a\gamma} < 1.45 \times 10^{-9}\text{ GeV}^{-1}$  (95% CL).

**Noble liquids:** Liquid argon (LAr) and liquid xenon (LXe) are employed as DM targets, while R&D on liquid helium is ongoing. We refer to Ref. [154] for a review of the liquid noble gas detector technology in low-energy physics, as well to *Section 36.4* of this *Review*. At present the best constraints on DM-nucleus interactions come from multi-tonne experiments using xenon: the LZ experiment at SURF, PandaX-4T at CJPL and XENONnT at LNGS. These experiments probe particle masses down to  $\sim 6$  GeV (when using both light and charge signals) and the SI DM-nucleon cross section down to  $9.2 \times 10^{-48}\text{ cm}^2$  (at 36 GeV). LAr experiments employ pulse shape discrimination (PSD) that allows for distinguishing between ER and NR events, at the expense of higher energy thresholds than in LXe. The DarkSide-50 TPC at LNGS (until 2019) sets a minimum upper limit on the SI, DM-nucleon cross-section of  $6 \times 10^{-43}\text{ cm}^2$  at 10 GeV, while the single-phase experiment DEAP-3600 at SNOLAB constrains the SI cross-section to values below  $3.9 \times 10^{-45}\text{ cm}^2$  at 100 GeV.

In noble liquids, sub-GeV DM particles can be searched for by observing inelastic, ER processes following a low-energy nuclear recoil: excitation and ionisation of the recoiling atom (the hypothetical Migdal effect) and a bremsstrahlung photon [155]. As an example, LUX and XENON1T constrain DM particle masses between (0.3–5) GeV via bremsstrahlung photons and Migdal electrons. Even lower masses are accessible when using the amplified, charge signal only, at the expense of giving up discrimination between ERs and NRs. XENON1T probed particle masses down to 60 MeV,

while DarkSide-50 published constraints on WIMP masses as low as 40 MeV. DM masses at the MeV-scale can also be probed by exploiting the scattering off electrons. PandaX-4T presented light DM searches with ionisation signals, with NR and ER energy thresholds of 0.77 keV and 0.07 keV, obtaining leading constraints in the mass range 40 MeV–100 GeV and 100 MeV–10 GeV for a heavy and light mediator, respectively [156]. DarkSide-50 set limits in the mass range (16 – 56) MeV and above 80 MeV for a heavy and light mediator, respectively [157]. Noble liquids TPCs also search for solar axions, galactic ALPs and dark photons. XENONnT set upper limits on the axion-electron coupling of  $2 \times 10^{-12}$  in the mass range (10<sup>-6</sup>–1) eV for solar axions, and probes couplings between  $(1 - 2) \times 10^{-14}$  in the mass range (1–10) keV for galactic ALPs [158]. DarkSide-50 probes ALP masses down to 0.03 keV with couplings in the range  $10^{-13} - 10^{-14}$  [157].

The next generation of liquefied noble gas detectors are in construction (DarkSide-20k) or at the design and R&D stage (Argo, DARWIN/XLZD, PandaX-xT). These will increase the sensitivity to various DM candidates by 1-2 orders of magnitude, with the ultimate goal of exploring the experimentally accessible parameter space, until the backgrounds from neutrinos will start dominating the event rates.

**Room temperature scintillators:** Several large DM experiments using high-purity NaI(Tl) crystals are acquiring data in various underground laboratories. Of these, DAMA/LIBRA at LNGS has the highest mass, 250 kg, and the largest exposure: 1.33 t y with an energy threshold of 1 keV and 2.46 t y with an energy threshold of 2 keV. It is the only experiment in the field that reported an annually modulated event rate with a statistical significance of  $12.9\sigma$  C.L. (20 annual cycles), with a modulation amplitude around 0.02 events/(kg d keV) in the energy region (1-4) keV. These findings were interpreted as due to DM interactions via nuclear or electronic recoils. The ANAIS experiment at Canfranc operates 112.5 kg of NaI(Tl) scintillators with an energy threshold of 1 keV and a background rate of 3.6 events/(kg d keV) in the (1-6) keV region. A blind analysis of 3 y of data, for an exposure of 314 kg y is consistent with an absence of modulation at  $3.3\sigma$ . The COSINE-100 experiment, located at the Yangyang Underground Laboratory in Korea, operates 106 kg of NaI(Tl) crystals in a liquid scintillator, with an energy threshold of keV and a background rate of 3.6 events/(kg d keV). Results from a 173 kg y exposure in the (1-6) keV energy range are consistent, at 68.3% C.L., with both the null hypothesis and DAMA/LIBRA’s best fit value in the same energy range. A larger exposure and a reduced energy threshold are required to test DAMA/LIBRA for  $3\sigma$  coverage. COSINE-200, under construction at the new, deeper underground laboratory Yemilab, will be a larger experiment with reduced backgrounds. The SABRE experiment plans to operate a total of 50 kg of NaI(Tl) crystals, focussing on reaching a background level of 0.1 events/(kg d keV), an order of magnitude below DAMA/LIBRA. Twin detectors will be installed at LNGS and at the Stawell Underground Physics Laboratory in the Southern hemisphere. While a DM-induced signal is expected to have the same phase in both hemispheres, seasonal or site-related effects would show different amplitudes and phases in the twin detectors. The COSINUS experiment, under construction at LNGS, will use NaI crystals operated as cryogenic scintillating calorimeters to differentiate between nuclear and electronic recoils based on the observation of phonon and light signals. The first phase aims for an exposure of 100 kg d, while the second phase aims to achieve, with 1000 kg d, a fully model-independent cross-check of a NR origin of the DAMA/LIBRA signal.

**Room temperature ionisation detectors:** Silicon charged-coupled devices (CCDs) are employed for low-mass DM searches, as well as for hidden photon searches in the eV-mass range. Ionisation events induced in bulk silicon of high-resistivity, fully depleted CCDs are observed with charge resolutions around  $1\text{--}2\text{ e}^-$  and extremely low leakage currents, at the level of few  $\text{e}^- \text{ mm}^{-2}\text{d}^{-1}$ . The position of an energy deposit is reconstructed in 3 dimensions and the particle type (electron, neutron, muon,  $\alpha$ -particles, etc) is reconstructed based on the recorded track pattern.

The DAMIC experiment at SNOLAB yielded new constraints on DM-electron scattering, and

on the hidden-photon kinetic mixing parameter in the mass range (1-30) eV with an exposure of 7.6 kg d and on low-mass WIMPs with an exposure of 11 kg d. The SENSEI projects employs the skipper technology to achieve single-electron sensitivity. A run with a 2 g detector in the MINOS cavern at Fermilab yielded world-leading constraints on DM-electron scattering for a large range of sub-GeV dark matter masses. The skipper technology is also employed in the next stage of the DAMIC programme, DAMIC-M at LSM, which plans for a kg-size mass. The goal is to achieve thresholds of 2-3 electrons and to probe the DM-nucleon cross-section down to  $\text{few} \times 10^{-43} \text{ cm}^2$  around 2-3 GeV and the DM-electron cross section down to  $2 \times 10^{-41} \text{ cm}^2$  at 10 MeV mass. DAMIC-M has operated first CCDs at LSM and achieved constraints on sub-GeV DM particles interacting with electrons in the mass range (0.53-1000) MeV, for an exposure of 85.23 g d.

The NEWS-G collaboration operates spherical proportional counters filled with a noble gas. Advantages of this technology are the low intrinsic electronic noise and a high amplification gain, allowing for low energy thresholds down to single-electron detection, and the possibility to use different light targets (He, Ne, etc). A 60 cm diameter chamber operated at LSM with a gas mixture of Ne + CH<sub>4</sub> (0.7%) at 3.1 bar, excluded SI, WIMP-nucleon cross sections above  $4.4 \times 10^{-37} \text{ cm}^2$  at 0.5 GeV after an exposure of 9.6 kg d with an energy threshold  $\sim 100$  eV. The next iteration, a 140-cm sphere detector made of very low radioactivity copper (few  $\mu\text{Bq}/\text{kg}$  of <sup>238</sup>U and <sup>232</sup>Th) has been installed at SNOLAB in 2021. The detector has recently started to acquire physics data, with a predicted background level of  $(5 \pm 2)$  events/(kg keV d) for sub-keV events.

**Superheated liquid detectors:** Investigation of the spin-dependent interaction channel calls for target nuclei with uneven total angular momentum. A particularly favourable candidate is <sup>19</sup>F, the spin of which is carried mostly by the unpaired proton, yielding a cross-section which is almost a factor of ten higher than of other employed nuclei with spin (e.g., <sup>23</sup>Na, <sup>73</sup>Ge, <sup>127</sup>I, <sup>129</sup>Xe, <sup>131</sup>Xe). Fluorine is part of the target of experiments using superheated liquids, such as the ones operated by the PICO collaboration. A search in the PICO-60 C<sub>3</sub>F<sub>6</sub> bubble chamber at SNOLAB with an exposure of 1404 kg d and an energy threshold of 2.45 keV, yielded the most stringent constraint on the DM-proton SD cross-section at  $3.2 \times 10^{-41} \text{ cm}^2$  for a 25 GeV particle mass. In construction at SNOLAB is PICO-500, a detector with 250 l of superheated freon (C<sub>3</sub>F<sub>8</sub>) contained between two quartz jars inside a pressure vessel filled with mineral oil, itself inside a tank of ultra-pure water.

**Directional detectors:** Detectors capable of measuring the direction of the recoiling nucleus would unequivocally confirm the Galactic origin of a signal and could probe the region below the neutrino floor [159, 160]. Because nuclear recoils have a range which is about 10 times smaller than the one of Compton recoils of the same energy, gaseous detectors have an excellent intrinsic background rejection if they can measure the range of events precisely. Several directional detectors are presently in operation, where a 1 m<sup>3</sup> detector has a typical mass of a few 100 g and can measure the sense of an incoming nuclear recoil above a few tens of keV. Cygnus is a proto-collaboration which coordinates the R&D efforts for gas based TPCs with 1 keV threshold. One of these is CYGNO, an experiment that aims to build a 1-m drift length gaseous TPC filled with a He:CF<sub>4</sub> 60:40 gas mixture at atmospheric pressure and room temperature at LNGS.

A new technique is based on fine-grained nuclear emulsions (solid-state detectors with silver halide crystals uniformly dispersed in a gelatine film, where each crystal works as a sensor for charged particles), as proposed by the NEWSdm collaboration. These act as target and nanometric tracking device, and the expected NR tracks are sub- $\mu\text{m}$  in size. Due to the small crystal size and larger number density, a superior spatial resolution compared to gaseous detectors is obtained. Simulations show that to reach the neutrino floor, exposures of 10 t y and 100 t y are required if a 30 nm and 50 nm threshold for detecting the track length is reached. This requires further R&D, since current emulsions allow for 100 nm tracking and target masses are around 1 kg, with 10 kg y exposures planned. A proposed approach for the directional detection of sub-GeV DM is to use

two-dimensional materials such as monolayer graphene [161], from which the DM particle can eject electrons. Their energy and direction, correlated with the direction of the incoming DM, can be measured for instance with the proposed PTOLEMY experiment.

**New techniques:** To probe light (sub-GeV) DM particles, either via scatters off electrons or via couplings to phonons, new techniques beyond the ones discussed above are proposed. The DM particle mass that can be accessed in DM-electron scattering in noble liquids and semiconductors is limited by the minimum ionisation/excitation energy and the size of the band gap, respectively (at the  $\sim$ eV-scale). To reach lower energy thresholds, materials with smaller band gaps for electron excitations ( $\sim$ meV), such as superconductors and superfluids, as well as Dirac materials were proposed [162]. These would in principle allow for the detection of keV-scale DM. Other ideas to detect keV-MeV scale DM are to observe NRs in superfluid He, via collective excitation modes in the fluid [163], as realised in HeRALD and DELight, or based on the breaking of chemical bonds between atoms [164].

Even lighter DM, with masses in the meV-eV range, could be detected via absorption on a conduction electron in a superconductor, followed by the emission of an athermal phonon [165]. Another proposed target for light DM are polar materials (for example GaAs, sapphire), which are especially sensitive for scattering through an ultralight dark photon, via excitation of single optical phonons [166]. If an anisotropic crystal such as sapphire is employed, a daily modulation interaction rate could be established [167]. A new class of detectors for bosonic DM, based on resonant absorption onto a gas of small polyatomic molecules, is proposed in [168]. The DM would effectively act as a laser that resonantly excites transitions in molecules when its mass closely matches the transition energy. While DM with SI couplings can efficiently excite phonons, it has been shown in [169] that if DM couples to the electron spin, magnon excitations (quanta of collective spin wave excitations) in materials with magnetic dipole order may also offer a promising detection avenue. Yet another approach for sub-GeV DM is to employ superconducting nanowires as both target and sensor, and first bounds on DM-electron interactions were placed from a 4.3 ng tungsten-silicide prototype with a 0.8 eV energy threshold and an exposure of  $8.8 \times 10^{-14}$  kg y [170].

The detection of light DM via collective excitations in condensed matter systems and other methods is a rapidly evolving field, and a growing area of research at the interface of DM physics, condensed matter and materials science. We refer to Ref. [171, 172] for discussions of some of these new directions and models. Critical challenges are to detect these very small energy depositions, and to reliably assess the background noise.

Table 27.1 summarises the most stringent constraints on the DM-nucleon SI and SD cross-sections, and Figure 27.1 shows the best constraints for SI couplings in the cross-section versus DM mass parameter space, above masses of 0.3 GeV.

## 27.7 Astrophysical detection of dark matter

DM as a microscopic constituent can have measurable, macroscopic effects on astrophysical systems. Indirect DM detection refers to the search for the annihilation or decay debris from DM particles, resulting in detectable species, including especially gamma rays, neutrinos, and antimatter particles. The production rate of such particles depends on (i) the annihilation (or decay) rate (ii) the density of pairs (respectively, of individual particles) in the region of interest, and (iii) the number of final-state particles produced in one annihilation (decay) event. In formulae, the rate for production of a final state particle  $f$  per unit volume from DM annihilation can be cast as

$$\Gamma_f^A = c \frac{\rho_{\text{DM}}^2}{m_{\text{DM}}^2} \langle \sigma v \rangle N_f^A, \quad (27.18)$$

where  $\langle\sigma v\rangle$  indicates the thermally-averaged cross section for DM annihilation times relative velocity [27], calculated at the appropriate temperature,  $\rho_{\text{DM}}$  is the physical density of DM, and  $N_f^A$  is the number of final state particles  $f$  produced in one individual annihilation event. The constant  $c$  depends on whether the DM is its own antiparticle, in which case  $c = 1/2$ , or if there is a mixture of DM particles and antiparticles (in case there is no asymmetry,  $c = 1/4$ ). The analog for decay is

$$\Gamma_f^D = \frac{\rho_{\text{DM}}}{m_{\text{DM}}} \frac{1}{\tau_{\text{DM}}} N_f^D, \quad (27.19)$$

with the same conventions for the symbols, and where  $\tau_{\text{DM}}$  is the DM's lifetime.

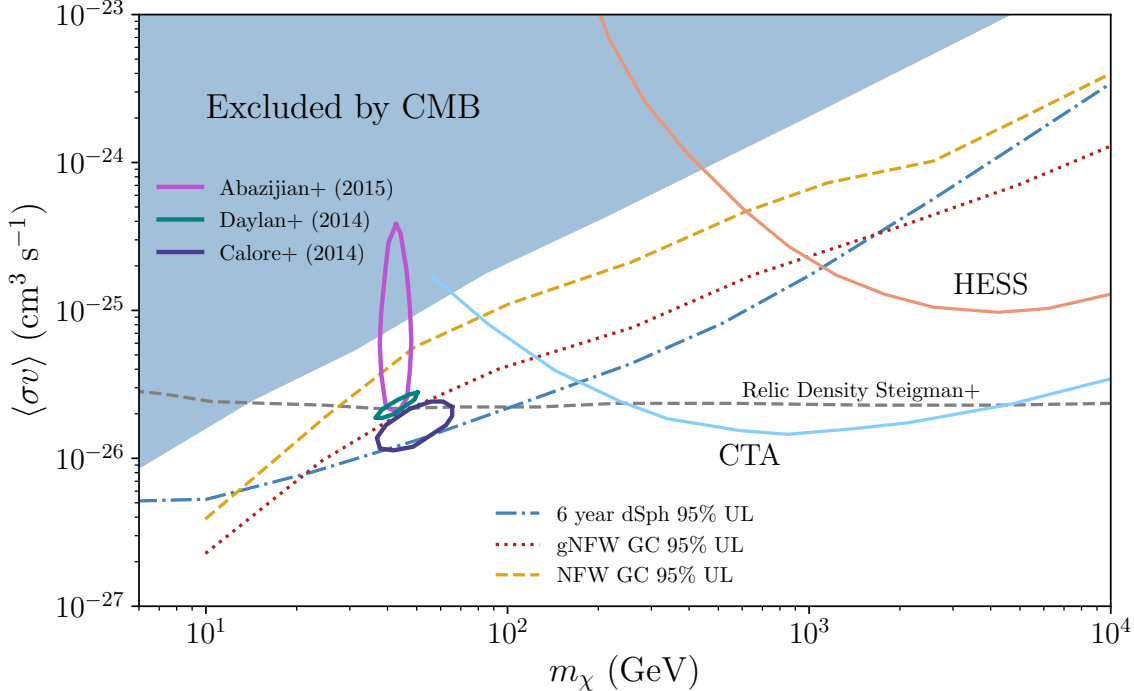


**Figure 27.2:** Upper limits and projected sensitivity from CTA on the pair-annihilation rate versus the DM mass from gamma-ray and CMB observations (figure courtesy of Logan Morrison).

**Gamma Rays:** DM annihilation to virtually any final state produces gamma rays: emission processes include the dominant two-photon decay mode of neutral pions resulting from the hadronization of strongly-interacting final states; final state radiation; and internal bremsstrahlung, the latter two including, possibly, the emission of massive gauge or Higgs bosons subsequently producing photons via their decay products. Similarly, neutrinos are produced from charged pion decay and from radiative processes. The flux of gamma rays and neutrinos is calculated integrating the rate  $\Gamma_f$  per steradian (simply meaning, for isotropic emission,  $\Gamma_f/(4\pi)$ ) along the line of sight within the appropriate angular region (the *differential* flux is obtained in the same way by simply replacing  $N_f$  with the differential flux at production, at the appropriate redshift in the case of cosmologically distant sources),

$$\phi_f = \int_{\Delta\Omega} d\Omega \int_{\text{l.o.s.}} dl \frac{\Gamma_f}{4\pi}. \quad (27.20)$$

It is customary to factor out, in the expression for the rate, a *particle physics* factor, depending upon the DM particle mass and its annihilation or decay rate, and an *astrophysical* factor, which only depends on the observational target. The latter is sometimes denoted with  $J_{\Delta\Omega}(\psi)$  with  $\psi$

indicating the direction of the line of sight. Although different conventions are in use, a common choice is to define

$$J_{\Delta\Omega}(\psi) = \int_{\Delta\Omega} \int_{\text{l.o.s.}(\psi)} \rho_{\text{DM}}^2(l, \Omega) \, dl d\Omega. \quad (27.21)$$

For a target with uniform density  $\rho$  and radius  $r$  at a distance  $d \gg r$ , such that the target is entirely within the solid angle  $\Delta\Omega$ ,

$$J \simeq \frac{4\pi r^3 \bar{\rho}_{\text{DM}}^2}{3d^2}. \quad (27.22)$$

Searches for gamma-ray emission from DM annihilation have focused on targets chosen based on a variety of considerations, primarily intended to maximize signal to noise. Nearby dwarf spheroidal galaxies contain very small amounts of gas, and do not host any significant astrophysical background at gamma-ray or X-ray frequencies, and are thus an optimal target choice for DM searches. An accurate determination of the DM density profile in these objects results in somewhat large systematics when deriving constraints from the non-observation of emission from DM; future optical surveys will help pinpoint with greater accuracy stellar kinematics and thus reduce such uncertainty; a second target is the inner region of the Milky Way: while nearby and potentially hosting a large density of DM, the Galactic center region is however very bright at almost any wavelength, making the extraction of a signal highly problematic; nearby clusters of galaxies are also known to host significant astrophysical emission, but are potentially ideally suited to constrain DM decay. Finally, putative nearby DM clumps are also a possible source of a bright DM signal (albeit from an unknown direction), as is the annihilation of DM in all halos at all redshifts.

DM annihilation and decay can lead to striking spectral features. Since the process happens typically at very low particle velocities, if the DM pair-annihilates e.g. to two photons or two neutrinos, the final-state particles will be nearly monoenergetic, with an energy close to the DM particle mass and a width proportional to the DM velocity in units of  $c$  (if a  $\gamma\gamma$  line is present electroweak symmetry also implies a  $Z\gamma$  line, if kinematically allowed). No astrophysical processes are known to produce lines at gamma-ray or neutrino energies in the GeV and above (with, perhaps, the possible exception of cold pulsar winds [173]) making this channel virtually background-free. At lower energy, lines are expected from radiative decay modes of candidates such as sterile neutrinos (see Sec. 27.5). DM annihilation or decay can lead to additional spectral features besides lines. These include (one or more) “boxes” [174], produced by boosted final states decaying to monochromatic photons (such as e.g. neutral pions), or combinations thereof. Processes occurring at higher redshift can distort these spectral features by smearing them to lower energies. Neglecting gamma-ray attenuation, the flux of gamma rays from all redshift can be cast as

$$\frac{dN_\gamma}{dE_\gamma}(E_\gamma) = \frac{c}{8\pi} \int \frac{\langle\sigma v\rangle \rho_{\text{DM}}(z) dz}{H(z)(1+z)^3 m_{\text{DM}}^2} \left( \frac{dN_\gamma}{dE'} \right)_{E'=E_\gamma(1+z)}. \quad (27.23)$$

While the calculation of the differential spectrum of gamma rays from a given final state  $f$ ,  $dN_\gamma^f/dE_\gamma$ , is carried out using numerical tools, such as PYTHIA [175] that reproduce hadronization and particle decay for masses well above a few GeV, in the sub-GeV range gamma-ray production follows primarily from meson decay and radiative processes well outside the range of applicability of the Altarelli-Parisi splitting function. The MeV gamma-ray range will soon be probed with forthcoming satellites [176]. Recently a code that provides the expected gamma-ray spectrum for sub-GeV DM, Hazma, has become available [177].

Observations with the Fermi Large Area Telescope (LAT) and with ground-based facilities such as HESS, VERITAS, MAGIC, and HAWC have provided an unprecedented picture of the gamma-ray sky ideally suited to look for a signal from DM annihilation or decay for DM particles from a few

GeV mass up to several TeV. The LAT has provided some of the most stringent constraints to-date on DM pair-annihilation for a variety of annihilation final states, chiefly from stacked observations of nearby satellite dwarf spheroidal galaxies [178]. Excesses of gamma rays over the expected diffuse and point-source background have been claimed, most importantly from the direction of the inner Galaxy, where a signal from DM annihilation might be especially bright [179, 180]. The nature of this excess is quite controversial: while the morphology and spectrum fall within what expected for a standard WIMP with a mass of a few tens of GeV [181], unresolved point sources, including especially an (expected) population of millisecond pulsars (MSPs) have been advocated as a possible plausible counterpart [182]. Statistical methods to discriminate between DM and MSPs have been utilized [183, 184], but recent studies indicate that such results might not be conclusive [185]. Large uncertainties in the Galactic diffuse background emission model are additionally known to exist, and possible plague the morphological and spectral information [186, 187]. Other notable potential gamma-ray excesses include a diffuse emission from the Andromeda galaxy (M31) [188–190], possibly in excess of what expected from cosmic-ray models [191]; and a diffuse emission at 511 keV energy in the inner Galaxy from Integral-SPI observations [192]; such emission has known astrophysical counterparts [193], as well as several proposed DM explanations (e.g. [194]).

While DM annihilation and decay typically occurs at low velocities, the possibility of “boosted” DM has also been considered [195]. In this case, the DM particle might dominantly pair-annihilate to a lighter dark species, which does interact with Standard Model particle, and could be detected with neutrino telescopes or direct detection experiments. Future facilities that promise to widen the reach of gamma-ray searches for DM include especially the Cherenkov Telescope Array (CTA), see fig. 27.2.

**Neutrinos:** DM can be captured in celestial bodies in significant amounts, depending on the DM scattering cross section off of nucleons, the DM mass, and the DM flux incident on the celestial body of interest. For DM masses at or around the GeV scale, evaporation from the celestial body plays an important role [196]. If enough DM accumulates, DM annihilation inside the celestial body can then lead to the production of Standard Model particles. Such particles can heat up the body, if they lose most of their energy before escaping. Utilizing models for heat production in planets, or stellar interior models in the case of stars, constraints can be put on DM particle properties. Of note are constraints from anomalous warming of cold planets such as Uranus [197], alterations to the stellar structure or the Sun’s seismic activity [198], and anomalous Earth heat flow [199]. Alternately, DM annihilation in celestial bodies can result in the production of particles that can escape the body. Within the Standard Model, the only such instance is annihilation to neutrinos, but, similarly to the boosted DM case the DM can annihilate to a (stable or unstable) dark-sector particles, whose decay or interactions can be detected on Earth [200, 201]. For direct annihilation to neutrinos, given the lower limit on the DM mass from evaporation, the typical neutrino energies usually exceed the energy of neutrinos from the Sun, the best target for this type of searches, making this a virtually background-free DM search. Significant neutrino fluxes can only be achieved, however, if near-equilibration is reached between the capture and annihilation rates. In turn, this requires large-enough DM-nucleon scattering cross sections, to-date very close to the limits from direct detection (see sec. 27.6). Only spin-dependent cross section, and capture in the Sun usually provide large-enough neutrino fluxes. IceCube and ANTARES searches for an anomalous flux of high-energy neutrinos from the Sun yielded null results, which can be interpreted as constraints on spin-dependent nucleon-DM interactions under the assumption of equilibration and of specific annihilation final states [202, 203]. Lower-threshold detectors, including DeepCore [204] and PINGU [205], can produce interesting limits on lower-mass DM candidates above the evaporation threshold.

**Cosmic-ray Antimatter:** Stable charged particles produced by decays of products of, or

directly from DM annihilation or decay, populate the cosmic radiation and are a prime target for indirect DM searches. To maximize signal to noise, searches focus on relatively rare particle species, such as positrons, antiprotons, and antinuclei. While in certain models the production of particles and antiparticles is not symmetric [206], generally DM annihilation or decay produces as many particles as antiparticles in the final state. Charged particles produced by DM propagate and lose energy prior to reaching detectors. The transport of charged particles is customarily carried out in the context of diffusion models such as the Galactic “leaky box” setup, see e.g. [207]. While progress in constraining the uncertain propagation and energy-loss processes has been steady with improved data from new detectors such as PAMELA [208] and AMS-02 [209], the calculation of the particle flux at Earth from that at production suffers from significant uncertainties [207].

An excess of high-energy positrons over the standard secondary production from inelastic cosmic-ray interactions has been firmly established by several experiments, most recently and with the highest statistics by AMS-02 [210]. The excess has been ascribed to DM annihilation, although strong constraints from the non-observation of corresponding anomalies in other channels, such as antiprotons and gamma rays, and the peculiar spectral shape, force DM models to be quite convoluted (see e.g. [211]). Alternately, excess *primary* positrons can be produced in the magnetosphere of nearby pulsars [212, 213]. This latter explanation was questioned in [214] in connection with the detection of a TeV halo around two candidate pulsars, leading to the determination of a highly suppressed diffusion coefficient within the pulsar nebula; with such low diffusion coefficient, positrons from the pulsars would not contribute significantly to the flux at Earth; Ref. [215], however, showed that likely the diffusion coefficient is not constant, and that if it increases outside the nebula, as expected from other cosmic-ray measurements, pulsars can still be considered as the counterpart to the positron excess. Other explanations for the excess, albeit somewhat controversial, and increasingly constrained by data, also exist [216, 217].

The antiproton spectrum in the cosmic radiation as measured by AMS-02 [209] also exhibits features that might be considered as excess flux between 10 and 20 GeV, and energies above 100 GeV [218], which have been interpreted as possible signal of DM annihilation; more realistically, however, systematic uncertainties in the antiproton production cross section, in cosmic-ray transport, reacceleration at high energy and, at low energy, solar modulation make it extremely difficult to assess the robustness of the excesses [219, 220].

Antinuclei such as anti-deuterium and anti-helium could also form as a result of DM annihilation or decay. While baryon number conservation forces the typical kinetic energy of antinuclei produced in inelastic cosmic-ray processes to large values, antinuclei arising from hadronization of DM-initiated jets have low energy, offering optimal signal-to-noise when a low-energy cut on the antinucleus kinetic energy is used [221–225]. Specific detector designs have been developed to single out low-energy cosmic-ray antinuclei (e.g.  $E < 0.25$  GeV/nucleon in the case of the General Antiparticle Spectrometer, or GAPS [226]). The detection of even a single antinucleus would have considerable importance as a possible sign of new physics [227].

**Multi-wavelength studies:** Electrons and positrons from DM lose energy quite efficiently, radiating at a variety of wavelengths. This *secondary* radiative emission presents spectral and morphological features that might provide an important additional indirect detection channel. The most efficient energy loss mechanisms for high-energy electrons and positrons are inverse Compton (IC) up-scattering of background photons, and synchrotron radiation in the presence of magnetic fields. Depending on the DM mass, the emitted light from synchrotron peaks at MHz-GHz frequencies, while the IC emission at X-ray to gamma-ray frequencies, depending on the energy of the background radiation, typically ranging from CMB photons up to starlight photons [228–230]. The calculation of the secondary emission from DM entails both solving the transport of the electrons and positrons from DM, and for the radiative emission; codes exist that perform these calculations

for certain astrophysical environments [231–233], with diffusion playing an increasingly critical role in smaller and smaller structures such as dwarf galaxies [229]. It has been demonstrated that for large magnetic fields and for certain final states, the synchrotron emission is more constraining than the gamma-ray emission [234].

**Stellar Physics:** Microscopic properties of the DM can meaningfully alter, and thus be constrained by, several astrophysical environments, from planets and stars, up to the universe as a whole. DM particles light enough to be produced in collisional processes inside stars, with typically temperatures in the keV, or supernovae, with energy scales in the MeV, lead to an additional energy-loss mechanism, if capable of escaping the system. If this is the case, the increased needed energy output would also result in an increased neutrino flux, leading to constraints on the masses and couplings of the DM, see e.g. [235] for a comprehensive review. DM annihilation can even have fueled early stages of stellar evolution, perhaps with measurable consequences [236]. DM capture in neutron stars could lead to the collapse of the star into black holes; the existence of neutron stars in DM-rich environments can thus be used to constrain the mass and interaction cross section of DM with nucleons [237] and even relatively light, but stable, primordial black holes [238].

**Cosmology:** Energy injection from DM processes in the early universe, as well as the contribution of DM to the effective relativistic degrees of freedom, are severely constrained from data on Big Bang Nucleosynthesis (see Sec. 24 in this *Review*) and on the energy and anisotropy power spectrum of the CMB (see Sec. 29). Codes exist that perform the calculation of the constraints on particle DM models [177, 239].

**PBH Detection:** Macroscopic DM candidates can gravitationally perturb structure and compromise the stability of, for instance, globular clusters such as Eridanus II [24], and/or disrupt wide binaries [240]. This constrains the maximal mass of a macroscopic DM candidate to not much more than  $5 M_\odot$  [240] (see also [24]). In the specific case of primordial black holes, strong constraints also stem from the acceleration of charged particles around and after recombination, with significant effects on the CMB [241], albeit a lively debate exists over the accretion efficiency around such objects at high redshift [242, 243]. Whether or not PBH in the solar-mass range can be 100% of the DM is therefore disputed at present. Other effects produced by macroscopic, massive DM candidates are the microlensing of stars [244, 245] and quasars [246], femtolensing of gamma-ray bursts [247], and neutron star capture [238]. It is important to note that recently constraints from both microlensing and femtolensing have been corrected after the realization of important finite-size source and wave effects [245, 248, 249], leaving a substantial window, at PBH masses  $10^{17} \lesssim M_{\text{BH}}/\text{g} \lesssim 10^{21}$  where PBH can be 100% of the DM. Light black holes,  $M_{\text{BH}} \lesssim 10^{17} \text{ g}$ , are also constrained by the non-detection of products of evaporation [250]; future MeV gamma-ray detectors are slated to significantly improve such constraints and to enable the direct detection of Hawking radiation [251]. If evaporation shuts down at or near the Planck scale, Planck-scale relic PBH are generally expected to carry electric charge and to be detectable with direct detection and neutrino experiments, or with paleo-detectors [252].

## References

- [1] J. D. Simon, arXiv e-prints arXiv:1901.05465 (2019), [[arXiv:1901.05465](#)].
- [2] P. Salucci, *Astron. Astrophys. Rev.* **27**, 1, 2 (2019), [[arXiv:1811.08843](#)].
- [3] S. W. Allen, A. E. Evrard and A. B. Mantz, *Ann. Rev. Astron. Astrophys.* **49**, 409 (2011), [[arXiv:1103.4829](#)].
- [4] N. A. Bahcall *et al.*, *ApJ* **541**, 1 (2000).
- [5] S. D. M. White, G. Efstathiou and C. S. Frenk, *Mon. Not. Roy. Astron. Soc.* **262**, 1023 (1993).

- [6] A. J. S. Hamilton and M. Tegmark, *Mon. Not. Roy. Astron. Soc.* **330**, 506 (2002), [[arXiv:astro-ph/0008392](#)].
- [7] B. Famaey and S. McGaugh, *Living Rev. Rel.* **15**, 10 (2012), [[arXiv:1112.3960](#)].
- [8] S. W. Randall *et al.*, *Astrophys. J.* **679**, 1173 (2008), [[arXiv:0704.0261](#)].
- [9] R. H. Sanders, *Int. J. Mod. Phys. D* **27**, 14, 14 (2018), [[arXiv:1805.06804](#)].
- [10] S. D. McDermott, H.-B. Yu and K. M. Zurek, *Phys. Rev. D* **83**, 063509 (2011), [[arXiv:1011.2907](#)].
- [11] D. A. Buote *et al.*, *Astrophys. J.* **577**, 183 (2002), [[arXiv:astro-ph/0205469](#)].
- [12] D. Harvey *et al.*, *Science* **347**, 1462 (2015), [[arXiv:1503.07675](#)].
- [13] S. Tulin and H.-B. Yu, *Phys. Rept.* **730**, 1 (2018), [[arXiv:1705.02358](#)].
- [14] D. N. Spergel and P. J. Steinhardt, *Phys. Rev. Lett.* **84**, 3760 (2000), [[arXiv:astro-ph/9909386](#)].
- [15] S. Tremaine and J. E. Gunn, *Phys. Rev. Lett.* **42**, 407 (1979), [,66(1979)].
- [16] L. Randall, J. Scholtz and J. Unwin, *Mon. Not. Roy. Astron. Soc.* **467**, 2, 1515 (2017), [[arXiv:1611.04590](#)].
- [17] R. Hlozek *et al.*, *Phys. Rev. D* **91**, 10, 103512 (2015), [[arXiv:1410.2896](#)].
- [18] E. Armengaud *et al.*, *Mon. Not. Roy. Astron. Soc.* **471**, 4, 4606 (2017), [[arXiv:1703.09126](#)].
- [19] M. Nori *et al.*, *Mon. Not. Roy. Astron. Soc.* **482**, 3, 3227 (2019), [[arXiv:1809.09619](#)].
- [20] B. Bozek *et al.*, *Mon. Not. Roy. Astron. Soc.* **450**, 1, 209 (2015), [[arXiv:1409.3544](#)].
- [21] H.-Y. Schive *et al.*, *Astrophys. J.* **818**, 1, 89 (2016), [[arXiv:1508.04621](#)].
- [22] E. O. Nadler *et al.*, *Astrophys. J.* **878**, 2, L32 (2019), [*Astrophys. J. Lett.* 878, 32(2019)], [[arXiv:1904.10000](#)].
- [23] M. A. Monroy-Rodríguez and C. Allen, *ApJ* **790**, 2, 159 (2014), [[arXiv:1406.5169](#)].
- [24] T. D. Brandt, *Astrophys. J.* **824**, 2, L31 (2016), [[arXiv:1605.03665](#)].
- [25] B. Audren *et al.*, *JCAP* **1412**, 12, 028 (2014), [[arXiv:1407.2418](#)].
- [26] M. Dutra *et al.*, *JCAP* **1803**, 037 (2018), [[arXiv:1801.05447](#)].
- [27] P. Gondolo and G. Gelmini, *Nucl. Phys.* **B360**, 145 (1991).
- [28] J. L. Feng and J. Kumar, *Phys. Rev. Lett.* **101**, 231301 (2008), [[arXiv:0803.4196](#)].
- [29] G. Jungman, M. Kamionkowski and K. Griest, *Phys. Rept.* **267**, 195 (1996), [[hep-ph/9506380](#)].
- [30] J. Edsjo *et al.*, *JCAP* **0304**, 001 (2003), [[hep-ph/0301106](#)].
- [31] G. Servant and T. M. P. Tait, *Nucl. Phys.* **B650**, 391 (2003), [[hep-ph/0206071](#)].
- [32] D. Hooper and S. Profumo, *Phys. Rept.* **453**, 29 (2007), [[hep-ph/0701197](#)].
- [33] K. Griest and D. Seckel, *Phys. Rev. D* **43**, 3191 (1991).
- [34] R. T. Co *et al.*, *JCAP* **1512**, 12, 024 (2015), [[arXiv:1506.07532](#)].
- [35] V. S. Rychkov and A. Strumia, *Phys. Rev. D* **75**, 075011 (2007), [[hep-ph/0701104](#)].
- [36] E. D. Carlson, M. E. Machacek and L. J. Hall, *Astrophys. J.* **398**, 43 (1992).
- [37] D. Pappadopulo, J. T. Ruderman and G. Trevisan, *Phys. Rev. D* **94**, 3, 035005 (2016), [[arXiv:1602.04219](#)].
- [38] Y. Hochberg *et al.*, *Phys. Rev. Lett.* **113**, 171301 (2014), [[arXiv:1402.5143](#)].

- [39] E. Kuflik *et al.*, Phys. Rev. Lett. **116**, 22, 221302 (2016), [arXiv:1512.04545].
- [40] W. B. Lin *et al.*, Phys. Rev. Lett. **86**, 954 (2001), [arXiv:astro-ph/0009003].
- [41] G. B. Gelmini and P. Gondolo, Phys. Rev. **D74**, 023510 (2006), [hep-ph/0602230].
- [42] M. Hindmarsh, R. Kirk and S. M. West, JCAP **1403**, 037 (2014), [arXiv:1311.1637].
- [43] T. Moroi and L. Randall, Nucl. Phys. **B570**, 455 (2000), [hep-ph/9906527].
- [44] P. Hut and K. A. Olive, Phys. Lett. **87B**, 144 (1979).
- [45] S. Nussinov, Phys. Lett. **165B**, 55 (1985).
- [46] K. M. Zurek, Phys. Rept. **537**, 91 (2014), [arXiv:1308.0338].
- [47] Y. B. Zel'dovich and I. D. Novikov, Soviet Ast. **10**, 602 (1967).
- [48] S. Hawking, Mon. Not. Roy. Astron. Soc. **152**, 75 (1971).
- [49] B. J. Carr, ApJ **201**, 1 (1975).
- [50] J. I. Read, J. Phys. **G41**, 063101 (2014), [arXiv:1404.1938].
- [51] T. Piffl *et al.*, Astron. Astrophys. **562**, A91 (2014), [arXiv:1309.4293].
- [52] L. Necib and T. Lin, Astrophys. J. **926**, 2, 189 (2022), [arXiv:2102.02211].
- [53] A. M. Green, J. Phys. **G44**, 8, 084001 (2017), [arXiv:1703.10102].
- [54] A. Helmi *et al.*, Nature **7729**, 985 (2018).
- [55] L. Necib, M. Lisanti and V. Belokurov (2018), [arXiv:1807.02519].
- [56] N. W. Evans, C. A. J. O'Hare and C. McCabe, Phys. Rev. **D99**, 2, 023012 (2019), [arXiv:1810.11468].
- [57] S. Pöder *et al.*, A&A **676**, A134 (2023).
- [58] J. S. Bullock and M. Boylan-Kolchin, Ann. Rev. Astron. Astrophys. **55**, 343 (2017), [arXiv:1707.04256].
- [59] J. Zavala and C. S. Frenk (2019), [arXiv:1907.11775].
- [60] L. V. Sales, A. Wetzel and A. Fattahi, Nature Astron. **6**, 8, 897 (2022), [arXiv:2206.05295].
- [61] I. M. E. Santos-Santos *et al.*, Mon. Not. Roy. Astron. Soc. **495**, 1, 58 (2020), [arXiv:1911.09116].
- [62] J. Madhani *et al.*, in “American Astronomical Society Meeting Abstracts,” volume 54 of *American Astronomical Society Meeting Abstracts*, 209.08 (2022).
- [63] M. Geha *et al.*, Astrophys. J. **847**, 1, 4 (2017), [arXiv:1705.06743].
- [64] P. van Dokkum *et al.*, Nature **605**, 7910, 435 (2022), [arXiv:2205.08552].
- [65] K. E. Andrade *et al.* (2019), [arXiv:1901.00507].
- [66] G. Servant, in “Particle dark matter,” 164–189 (2010).
- [67] L. Hui *et al.*, Phys. Rev. **D95**, 4, 043541 (2017), [arXiv:1610.08297].
- [68] A. Fattahi *et al.* (2016), [arXiv:1607.06479].
- [69] D. J. E. Marsh, Phys. Rept. **643**, 1 (2016), [arXiv:1510.07633].
- [70] H. An *et al.*, Phys. Lett. **B747**, 331 (2015), [arXiv:1412.8378].
- [71] P. W. Graham and S. Rajendran, Phys. Rev. **D88**, 035023 (2013), [arXiv:1306.6088].
- [72] P. W. Graham *et al.*, Phys. Rev. **D93**, 7, 075029 (2016), [arXiv:1512.06165].
- [73] A. Arvanitaki *et al.*, Phys. Rev. **D97**, 7, 075020 (2018), [arXiv:1606.04541].
- [74] P. W. Graham *et al.*, Phys. Rev. **D97**, 5, 055006 (2018), [arXiv:1709.07852].

- [75] I. M. Bloch *et al.* (2019), [[arXiv:1907.03767](#)].
- [76] A. Pierce, K. Riles and Y. Zhao, *Phys. Rev. Lett.* **121**, 6, 061102 (2018), [[arXiv:1801.10161](#)].
- [77] Y. Kahn, B. R. Safdi and J. Thaler, *Phys. Rev. Lett.* **117**, 14, 141801 (2016), [[arXiv:1602.01086](#)].
- [78] R. Henning *et al.* (ABRACADABRA), in “Proceedings, 13th Patras Workshop on Axions, WIMPs and WISPs, (PATRAS 2017): Thessaloniki, Greece, 15 May 2017 - 19, 2017,” 28–31 (2018).
- [79] S. Chaudhuri *et al.*, *Phys. Rev.* **D92**, 7, 075012 (2015), [[arXiv:1411.7382](#)].
- [80] P. Sikivie, N. Sullivan and D. B. Tanner, *Phys. Rev. Lett.* **112**, 13, 131301 (2014), [[arXiv:1310.8545](#)].
- [81] B. M. Brubaker *et al.*, *Phys. Rev.* **D96**, 12, 123008 (2017), [[arXiv:1706.08388](#)].
- [82] G. Rybka (ADMX), *Phys. Dark Univ.* **4**, 14 (2014).
- [83] S. Dodelson and L. M. Widrow, *Phys. Rev. Lett.* **72**, 17 (1994), [[hep-ph/9303287](#)].
- [84] E. Bulbul *et al.*, *Astrophys. J.* **789**, 13 (2014), [[arXiv:1402.2301](#)].
- [85] A. Boyarsky *et al.*, *Phys. Rev. Lett.* **113**, 251301 (2014), [[arXiv:1402.4119](#)].
- [86] T. E. Jeltema and S. Profumo, *Mon. Not. Roy. Astron. Soc.* **450**, 2, 2143 (2015), [[arXiv:1408.1699](#)].
- [87] M. E. Anderson, E. Churazov and J. N. Bregman, *Mon. Not. Roy. Astron. Soc.* **452**, 4, 3905 (2015), [[arXiv:1408.4115](#)].
- [88] D. Malyshev, A. Neronov and D. Eckert, *Phys. Rev.* **D90**, 103506 (2014), [[arXiv:1408.3531](#)].
- [89] T. E. Jeltema and S. Profumo, *Mon. Not. Roy. Astron. Soc.* **458**, 4, 3592 (2016), [[arXiv:1512.01239](#)].
- [90] F. A. Aharonian *et al.* (Hitomi), *Astrophys. J.* **837**, 1, L15 (2017), [[arXiv:1607.07420](#)].
- [91] I. Yu. Kobzarev, L. B. Okun and I. Ya. Pomeranchuk, *Sov. J. Nucl. Phys.* **3**, 6, 837 (1966), [*Yad. Fiz.* **3**, 1154 (1966)].
- [92] M. J. Strassler and K. M. Zurek, *Phys. Lett.* **B651**, 374 (2007), [[hep-ph/0604261](#)].
- [93] M. J. Strassler (2006), [[hep-ph/0607160](#)].
- [94] M. Battaglieri *et al.*, in “U.S. Cosmic Visions: New Ideas in Dark Matter,” (2017), [[arXiv:1707.04591](#)].
- [95] Y. Kahn *et al.*, *JHEP* **05**, 002 (2017), [[arXiv:1609.09072](#)].
- [96] J. Alexander *et al.* (2016), [[arXiv:1608.08632](#)], URL <http://lss.fnal.gov/archive/2016/conf/fermilab-conf-16-421.pdf>.
- [97] K. R. Dienes and B. Thomas, *Phys. Rev.* **D85**, 083523 (2012), [[arXiv:1106.4546](#)].
- [98] N. Trevisani (ATLAS, CMS), *Universe* **4**, 11, 131 (2018).
- [99] E. Tolley (ATLAS), *PoS ICHEP2018*, 171 (2019).
- [100] W. C. Kalderon (ATLAS), *PoS DIS2018*, 085 (2018).
- [101] D. Vannerom (CMS), *PoS DIS2019*, 111 (2019).
- [102] G. Gómez-Ceballos (CMS), *PoS EDSU2018*, 014 (2018).
- [103] J. Aalbers *et al.* (LUX-ZEPLIN), *Phys. Rev. Lett.* **131**, 4, 041002 (2023), [[arXiv:2207.03764](#)].
- [104] Y. Meng *et al.* (PandaX-4T), *Phys. Rev. Lett.* **127**, 26, 261802 (2021), [[arXiv:2107.13438](#)].
- [105] E. Aprile *et al.* (XENON), *Phys. Rev. Lett.* **131**, 4, 041003 (2023), [[arXiv:2303.14729](#)].

- [106] R. Agnese *et al.* (SuperCDMS), Phys. Rev. Lett. **120**, 6, 061802 (2018), [arXiv:1708.08869].
- [107] P. Agnes *et al.* (DarkSide-50), Phys. Rev. D **107**, 6, 063001 (2023), [arXiv:2207.11966].
- [108] R. Ajaj *et al.* (DEAP), Phys. Rev. D **100**, 022004 (2019), [arXiv:1902.04048].
- [109] D. S. Akerib *et al.* (LUX), Phys. Rev. Lett. **122**, 13, 131301 (2019), [arXiv:1811.11241].
- [110] E. Aprile *et al.* (XENON) (2019), [arXiv:1907.12771].
- [111] E. Aprile *et al.* (2019), [arXiv:1907.11485].
- [112] R. Agnese *et al.* (SuperCDMS), Phys. Rev. D **99**, 6, 062001 (2019), [arXiv:1808.09098].
- [113] M. F. Albakry *et al.* (SuperCDMS), Phys. Rev. D **107**, 11, 112013 (2023), [arXiv:2302.09115].
- [114] A. H. Abdelhameed *et al.* (CRESST) (2019), [arXiv:1904.00498].
- [115] G. Angloher *et al.* (CRESST), Phys. Rev. D **107**, 12, 122003 (2023), [arXiv:2212.12513].
- [116] A. Aguilar-Arevalo *et al.* (DAMIC), Phys. Rev. Lett. **125**, 241803 (2020), [arXiv:2007.15622].
- [117] Q. Arnaud *et al.* (NEWS-G), Astropart. Phys. **97**, 54 (2018), [arXiv:1706.04934].
- [118] C. Amole *et al.* (PICO), Phys. Rev. D **100**, 2, 022001 (2019), [arXiv:1902.04031].
- [119] Z. Huang *et al.* (PandaX), Phys. Lett. B **834**, 137487 (2022), [arXiv:2208.03626].
- [120] J. D. Lewin and P. F. Smith, Astropart. Phys. **6**, 87 (1996).
- [121] J. R. Ellis, R. A. Flores and J. D. Lewin, Phys. Lett. **B212**, 375 (1988).
- [122] P. J. Fox, J. Liu and N. Weiner, Phys. Rev. D **83**, 103514 (2011), [arXiv:1011.1915].
- [123] L. Vietze *et al.*, Phys. Rev. D **91**, 4, 043520 (2015), [arXiv:1412.6091].
- [124] B. S. Hu *et al.*, Phys. Rev. Lett. **128**, 7, 072502 (2022), [arXiv:2109.00193].
- [125] J. Ellis, N. Nagata and K. A. Olive, Eur. Phys. J. **C78**, 7, 569 (2018), [arXiv:1805.09795].
- [126] J. Fan, M. Reece and L.-T. Wang, JCAP **1011**, 042 (2010), [arXiv:1008.1591].
- [127] A. L. Fitzpatrick *et al.*, JCAP **1302**, 004 (2013), [arXiv:1203.3542].
- [128] N. Anand, A. L. Fitzpatrick and W. C. Haxton, Phys. Rev. C **89**, 6, 065501 (2014), [arXiv:1308.6288].
- [129] M. I. Gresham and K. M. Zurek, Phys. Rev. D **89**, 12, 123521 (2014), [arXiv:1401.3739].
- [130] J. B. Dent *et al.*, Phys. Rev. D **92**, 6, 063515 (2015), [arXiv:1505.03117].
- [131] D. Gazda, R. Catena and C. Forssén, Phys. Rev. D **95**, 10, 103011 (2017), [arXiv:1612.09165].
- [132] M. Hoferichter *et al.*, Phys. Rev. D **99**, 5, 055031 (2019), [arXiv:1812.05617].
- [133] R. Essig, J. Mardon and T. Volansky, Phys. Rev. D **85**, 076007 (2012), [arXiv:1108.5383].
- [134] R. Catena *et al.*, JCAP **03**, 052 (2023), [arXiv:2210.07305].
- [135] T. Trickle, Phys. Rev. D **107**, 3, 035035 (2023), [arXiv:2210.14917].
- [136] F. T. Avignone, III *et al.*, Phys. Rev. D **35**, 2752 (1987).
- [137] M. Pospelov, A. Ritz and M. B. Voloshin, Phys. Rev. D **78**, 115012 (2008), [arXiv:0807.3279].
- [138] I. M. Bloch *et al.*, JHEP **06**, 087 (2017), [arXiv:1608.02123].
- [139] Y. Hochberg, T. Lin and K. M. Zurek, Phys. Rev. D **95**, 2, 023013 (2017), [arXiv:1608.01994].
- [140] M. Schumann, J. Phys. G **46**, 10, 103003 (2019), [arXiv:1903.03026].
- [141] J. Billard *et al.*, Rept. Prog. Phys. **85**, 5, 056201 (2022), [arXiv:2104.07634].
- [142] M. Pato *et al.*, Phys. Rev. D **83**, 083505 (2011), [arXiv:1012.3458].
- [143] A. K. Drukier, K. Freese and D. N. Spergel, Phys. Rev. D **33**, 3495 (1986).

- [144] D. N. Spergel, Phys. Rev. **D37**, 1353 (1988).
- [145] D. Stiff, L. M. Widrow and J. Frieman, Phys. Rev. **D64**, 083516 (2001), [arXiv:astro-ph/0106048].
- [146] K. Freese *et al.*, Phys. Rev. Lett. **92**, 111301 (2004), [arXiv:astro-ph/0310334].
- [147] T. Bruch *et al.*, Astrophys. J. **696**, 920 (2009), [arXiv:0804.2896].
- [148] M. J. Lewis and K. Freese, Phys. Rev. **D70**, 043501 (2004), [arXiv:astro-ph/0307190].
- [149] F. Mayet *et al.*, Phys. Rept. **627**, 1 (2016), [arXiv:1602.03781].
- [150] L. E. Strigari, New J. Phys. **11**, 105011 (2009), [arXiv:0903.3630].
- [151] C. A. J. O'Hare, Phys. Rev. Lett. **127**, 25, 251802 (2021), [arXiv:2109.03116].
- [152] L. E. Strigari, Phys. Rev. **D93**, 10, 103534 (2016), [arXiv:1604.00729].
- [153] R. Essig, M. Sholapurkar and T.-T. Yu, Phys. Rev. **D97**, 9, 095029 (2018), [arXiv:1801.10159].
- [154] V. Chepel and H. Araujo, JINST **8**, R04001 (2013), [arXiv:1207.2292].
- [155] M. J. Dolan, F. Kahlhoefer and C. McCabe, Phys. Rev. Lett. **121**, 10, 101801 (2018), [arXiv:1711.09906].
- [156] S. Li *et al.* (PandaX), Phys. Rev. Lett. **130**, 26, 261001 (2023), [arXiv:2212.10067].
- [157] P. Agnes *et al.* (DarkSide), Phys. Rev. Lett. **130**, 10, 101002 (2023), [arXiv:2207.11968].
- [158] E. Aprile *et al.* (XENON), Phys. Rev. Lett. **129**, 16, 161805 (2022), [arXiv:2207.11330].
- [159] P. Grothaus, M. Fairbairn and J. Monroe, Phys. Rev. **D90**, 5, 055018 (2014), [arXiv:1406.5047].
- [160] C. A. J. O'Hare *et al.*, Phys. Rev. **D92**, 6, 063518 (2015), [arXiv:1505.08061].
- [161] Y. Hochberg *et al.*, Phys. Lett. **B772**, 239 (2017), [arXiv:1606.08849].
- [162] Y. Hochberg *et al.*, Phys. Rev. **D97**, 1, 015004 (2018), [arXiv:1708.08929].
- [163] S. Knapen, T. Lin and K. M. Zurek, Phys. Rev. **D95**, 5, 056019 (2017), [arXiv:1611.06228].
- [164] R. Essig *et al.*, Phys. Rev. **D95**, 5, 056011 (2017), [arXiv:1608.02940].
- [165] Y. Hochberg, T. Lin and K. M. Zurek, Phys. Rev. **D94**, 1, 015019 (2016), [arXiv:1604.06800].
- [166] S. Knapen *et al.*, Phys. Lett. **B785**, 386 (2018), [arXiv:1712.06598].
- [167] S. Griffin *et al.*, Phys. Rev. **D98**, 11, 115034 (2018), [arXiv:1807.10291].
- [168] A. Arvanitaki, S. Dimopoulos and K. Van Tilburg, Phys. Rev. **X8**, 4, 041001 (2018), [arXiv:1709.05354].
- [169] T. Trickle, Z. Zhang and K. M. Zurek (2019), [arXiv:1905.13744].
- [170] Y. Hochberg *et al.*, Phys. Rev. D **106**, 11, 112005 (2022), [arXiv:2110.01586].
- [171] T. Lin, PoS **333**, 009 (2019), [arXiv:1904.07915].
- [172] R. Essig *et al.*, in “Snowmass 2021,” (2022), [arXiv:2203.08297].
- [173] F. Aharonian, D. Khangulyan and D. Malyshev, Astron. Astrophys. **547**, A114 (2012), [arXiv:1207.0458].
- [174] K. K. Boddy *et al.*, Phys. Rev. **D94**, 9, 095027 (2016), [arXiv:1606.07440].
- [175] T. Sjöstrand (2019), [arXiv:1907.09874].
- [176] M. Tavani *et al.* (e-ASTROGAM), JHEAp **19**, 1 (2018), [arXiv:1711.01265].
- [177] A. Coogan, L. Morrison and S. Profumo (2019), [arXiv:1907.11846].

- [178] M. Ackermann *et al.* (Fermi-LAT), Phys. Rev. Lett. **115**, 23, 231301 (2015), [[arXiv:1503.02641](#)].
- [179] D. Hooper and L. Goodenough, Phys. Lett. **B697**, 412 (2011), [[arXiv:1010.2752](#)].
- [180] M. Ackermann *et al.* (Fermi-LAT), Astrophys. J. **840**, 1, 43 (2017), [[arXiv:1704.03910](#)].
- [181] F. Calore, I. Cholis and C. Weniger, JCAP **1503**, 038 (2015), [[arXiv:1409.0042](#)].
- [182] K. N. Abazajian and M. Kaplinghat, Phys. Rev. **D86**, 083511 (2012), [Erratum: Phys. Rev. **D87**, 129902 (2013)], [[arXiv:1207.6047](#)].
- [183] S. K. Lee, M. Lisanti and B. R. Safdi, JCAP **1505**, 05, 056 (2015), [[arXiv:1412.6099](#)].
- [184] T. Daylan *et al.*, Phys. Dark Univ. **12**, 1 (2016), [[arXiv:1402.6703](#)].
- [185] R. K. Leane and T. R. Slatyer (2019), [[arXiv:1904.08430](#)].
- [186] E. Carlson, T. Linden and S. Profumo, Phys. Rev. Lett. **117**, 11, 111101 (2016), [[arXiv:1510.04698](#)].
- [187] M. Ajello *et al.* (Fermi-LAT), Astrophys. J. **819**, 1, 44 (2016), [[arXiv:1511.02938](#)].
- [188] M. Ackermann *et al.* (Fermi-LAT), Astrophys. J. **836**, 2, 208 (2017), [[arXiv:1702.08602](#)].
- [189] A. McDaniel, T. Jeltema and S. Profumo, Phys. Rev. **D97**, 10, 103021 (2018), [[arXiv:1802.05258](#)].
- [190] C. Karwin *et al.* (2019), [[arXiv:1903.10533](#)].
- [191] A. McDaniel, T. Jeltema and S. Profumo, Phys. Rev. **D100**, 2, 023014 (2019), [[arXiv:1903.06833](#)].
- [192] R. L. Kinzer *et al.*, Astrophys. J. **559**, 282 (2001).
- [193] R. M. Bandyopadhyay *et al.*, Mon. Not. Roy. Astron. Soc. **392**, 1115 (2009), [[arXiv:0810.3674](#)].
- [194] D. P. Finkbeiner and N. Weiner, Phys. Rev. **D76**, 083519 (2007), [[arXiv:astro-ph/0702587](#)].
- [195] K. Agashe *et al.*, JCAP **1410**, 10, 062 (2014), [[arXiv:1405.7370](#)].
- [196] T. Damour and L. M. Krauss, Phys. Rev. Lett. **81**, 5726 (1998), [[arXiv:astro-ph/9806165](#)].
- [197] S. L. Adler, Phys. Lett. **B671**, 203 (2009), [[arXiv:0808.2823](#)].
- [198] J. Casanellas and I. Lopes, Astrophys. J. **765**, L21 (2013), [[arXiv:1212.2985](#)].
- [199] G. D. Mack, J. F. Beacom and G. Bertone, Phys. Rev. **D76**, 043523 (2007), [[arXiv:0705.4298](#)].
- [200] J. Smolinsky and P. Tanedo, Phys. Rev. **D95**, 7, 075015 (2017), [Erratum: Phys. Rev.D96,no.9,099902(2017)], [[arXiv:1701.03168](#)].
- [201] C. Niblaeus, A. Beniwal and J. Edsjo (2019), [[arXiv:1903.11363](#)].
- [202] M. G. Aartsen *et al.* (IceCube), JCAP **1604**, 04, 022 (2016), [[arXiv:1601.00653](#)].
- [203] S. Adrian-Martinez *et al.* (ANTARES), Phys. Lett. **B759**, 69 (2016), [[arXiv:1603.02228](#)].
- [204] C. R. Das *et al.*, Phys. Lett. **B725**, 297 (2013), [[arXiv:1110.5095](#)].
- [205] M. G. Aartsen *et al.* (IceCube), J. Phys. **G44**, 5, 054006 (2017), [[arXiv:1607.02671](#)].
- [206] Y. Zhao and K. M. Zurek, JHEP **07**, 017 (2014), [[arXiv:1401.7664](#)].
- [207] A. W. Strong, I. V. Moskalenko and V. S. Ptuskin, Ann. Rev. Nucl. Part. Sci. **57**, 285 (2007), [[arXiv:astro-ph/0701517](#)].
- [208] O. Adriani *et al.* (PAMELA), Phys. Rev. Lett. **111**, 081102 (2013), [[arXiv:1308.0133](#)].
- [209] M. Aguilar *et al.* (AMS), Phys. Rev. Lett. **117**, 9, 091103 (2016).
- [210] M. Aguilar *et al.* (AMS), Phys. Rev. Lett. **110**, 141102 (2013).

- [211] S. Profumo, F. Queiroz and C. Siqueira (2019), [[arXiv:1903.07638](#)].
- [212] D. Hooper, P. Blasi and P. D. Serpico, *JCAP* **0901**, 025 (2009), [[arXiv:0810.1527](#)].
- [213] S. Profumo, *Central Eur. J. Phys.* **10**, 1 (2011), [[arXiv:0812.4457](#)].
- [214] A. U. Abeysekara *et al.* (HAWC), *Science* **358**, 6365, 911 (2017), [[arXiv:1711.06223](#)].
- [215] S. Profumo *et al.*, *Phys. Rev.* **D97**, 12, 123008 (2018), [[arXiv:1803.09731](#)].
- [216] R. Cowsik, B. Burch and T. Madziwa-Nussinov, *Astrophys. J.* **786**, 124 (2014), [[arXiv:1305.1242](#)].
- [217] K. Blum, B. Katz and E. Waxman, *Phys. Rev. Lett.* **111**, 21, 211101 (2013), [[arXiv:1305.1324](#)].
- [218] M.-Y. Cui *et al.*, *Phys. Rev. Lett.* **118**, 19, 191101 (2017), [[arXiv:1610.03840](#)].
- [219] A. Reinert and M. W. Winkler, *JCAP* **1801**, 01, 055 (2018), [[arXiv:1712.00002](#)].
- [220] M. W. Winkler, *JCAP* **1702**, 02, 048 (2017), [[arXiv:1701.04866](#)].
- [221] F. Donato, N. Fornengo and P. Salati, *Phys. Rev.* **D62**, 043003 (2000), [[hep-ph/9904481](#)].
- [222] K. Mori *et al.*, *Astrophys. J.* **566**, 604 (2002), [[arXiv:astro-ph/0109463](#)].
- [223] H. Baer and S. Profumo, *JCAP* **0512**, 008 (2005), [[arXiv:astro-ph/0510722](#)].
- [224] E. Carlson *et al.*, *Phys. Rev.* **D89**, 7, 076005 (2014), [[arXiv:1401.2461](#)].
- [225] M. Cirelli *et al.*, *JHEP* **08**, 009 (2014), [[arXiv:1401.4017](#)].
- [226] R. Bird *et al.*, in “36th International Cosmic Ray Conference (ICRC 2019) Madison, Wisconsin, USA, July 24-August 1, 2019,” (2019), [[arXiv:1908.03154](#)].
- [227] A. Coogan and S. Profumo, *Phys. Rev.* **D96**, 8, 083020 (2017), [[arXiv:1705.09664](#)].
- [228] S. Colafrancesco, S. Profumo and P. Ullio, *Astron. Astrophys.* **455**, 21 (2006), [[arXiv:astro-ph/0507575](#)].
- [229] S. Colafrancesco, S. Profumo and P. Ullio, *Phys. Rev.* **D75**, 023513 (2007), [[arXiv:astro-ph/0607073](#)].
- [230] S. Profumo and P. Ullio (2010), [[arXiv:1001.4086](#)].
- [231] T. E. Jeltema and S. Profumo, *JCAP* **0811**, 003 (2008), [[arXiv:0808.2641](#)].
- [232] M. Cirelli *et al.*, *JCAP* **1103**, 051 (2011), [Erratum: *JCAP* 1210, E01(2012)], [[arXiv:1012.4515](#)].
- [233] A. McDaniel *et al.*, *JCAP* **1709**, 09, 027 (2017), [[arXiv:1705.09384](#)].
- [234] E. Storm *et al.*, *Astrophys. J.* **768**, 106 (2013), [[arXiv:1210.0872](#)].
- [235] G. G. Raffelt, *Stars as laboratories for fundamental physics* (1996), ISBN 9780226702728, URL <http://wwwth.mpp.mpg.de/members/raffelt/mypapers/199613.pdf>.
- [236] D. Spolyar, K. Freese and P. Gondolo, *Phys. Rev. Lett.* **100**, 051101 (2008), [[arXiv:0705.0521](#)].
- [237] S. Dimopoulos, J. Preskill and F. Wilczek, *Phys. Lett.* **119B**, 320 (1982).
- [238] P. Pani and A. Loeb, *JCAP* **1406**, 026 (2014), [[arXiv:1401.3025](#)].
- [239] H. Liu, G. W. Ridgway and T. R. Slatyer (2019), [[arXiv:1904.09296](#)].
- [240] M. A. Monroy-Rodríguez and C. Allen, *Astrophys. J.* **790**, 2, 159 (2014), [[arXiv:1406.5169](#)].
- [241] M. Ricotti, J. P. Ostriker and K. J. Mack, *Astrophys. J.* **680**, 829 (2008), [[arXiv:0709.0524](#)].
- [242] S. Bird *et al.*, *Phys. Rev. Lett.* **116**, 20, 201301 (2016), [[arXiv:1603.00464](#)].
- [243] V. Poulin *et al.*, *Phys. Rev.* **D96**, 8, 083524 (2017), [[arXiv:1707.04206](#)].

- [244] P. Tisserand *et al.* (EROS-2), *Astron. Astrophys.* **469**, 387 (2007), [[arXiv:astro-ph/0607207](#)].
- [245] H. Niikura *et al.*, *Nat. Astron.* **3**, 6, 524 (2019), [[arXiv:1701.02151](#)].
- [246] E. Mediavilla *et al.*, *Astrophys. J.* **706**, 1451 (2009), [[arXiv:0910.3645](#)].
- [247] A. Barnacka, J. F. Glicenstein and R. Moderski, *Phys. Rev.* **D86**, 043001 (2012), [[arXiv:1204.2056](#)].
- [248] A. Katz *et al.*, *JCAP* **1812**, 005 (2018), [[arXiv:1807.11495](#)].
- [249] N. Smyth *et al.* (2019), [[arXiv:1910.01285](#)].
- [250] B. J. Carr *et al.*, *Phys. Rev.* **D81**, 104019 (2010), [[arXiv:0912.5297](#)].
- [251] A. Coogan, L. Morrison and S. Profumo, *Phys. Rev. Lett.* **126**, 17, 171101 (2021), [[arXiv:2010.04797](#)].
- [252] B. V. Lehmann *et al.*, *JCAP* **10**, 046 (2019), [[arXiv:1906.06348](#)].